Modulation of electrical conduction through individual molecules on silicon by the electrostatic fields of nearby polar molecules: Theory and experiment

George Kirczenow,[1,2] Paul G. Piva,[3,*] and Robert A. Wolkow[2,3]
[1]*Department of Physics, Simon Fraser University, Burnaby, British Columbia, Canada V5A 1S6*
[2]*Nanoelectronics Program, The Canadian Institute for Advanced Research, Toronto, Ontario, Canada M5G 1Z8*
[3]*National Institute for Nanotechnology, National Research Council of Canada, Edmonton, Alberta, Canada T6G 2V4 and Department of Physics, University of Alberta, Edmonton, Alberta, Canada T6G 2J1*
(Received 17 December 2008; revised manuscript received 1 May 2009; published 14 July 2009)

We report on the synthesis, scanning tunneling microscopy (STM) and theoretical modeling of the electrostatic and transport properties of one-dimensional organic heterostructures consisting of contiguous lines of CF_3- and OCH_3-substituted styrene molecules on silicon. The electrostatic fields emanating from these polar molecules are found, under appropriate conditions, to strongly influence electrical conduction through nearby molecules and the underlying substrate. For suitable alignment of the OCH_3 groups of the OCH_3-styrene molecules in the molecular chain, their combined electric fields are shown by *ab initio* density-functional calculations to give rise to potential profiles along the OCH_3-styrene chain that result in strongly enhanced conduction through OCH_3-styrene molecules near the heterojunction for moderately low negative substrate bias, as is observed experimentally. Under similar bias conditions, dipoles associated with the CF_3 groups are found in both experiment and in theory to depress transport in the underlying silicon. Under positive substrate bias, simulations suggest that the differing structural and electrostatic properties of the CF_3-styrene molecules may lead to a more sharply localized conduction enhancement near the heterojunction at low temperatures. Thus choice of substituents, their attachment site on the host styrene molecules on silicon and the orientations of the molecular dipole and higher multipole moments provide a means of differentially tuning transport on the molecular scale.

DOI: 10.1103/PhysRevB.80.035309 PACS number(s): 31.70.−f, 68.37.Ef, 68.43.−h, 73.63.−b

I. INTRODUCTION

During the last decade a great deal of research has focused on electrical conduction through individual molecules.[1–3] Many molecules are electrically polarized due to chemical charge transfer between unlike atoms. This results in electric fields that should influence electrical conduction through such molecules and through molecules in their vicinity. However, there have been few direct experimental investigations of such effects in the context of molecular-scale nanoelectronics. Recently experimental studies of the effects of charged chemical species attached to a molecule on electrical conduction through the *same* molecule have been reported.[4,5] The presence of a charged dangling bond on a silicon surface has been observed to affect electrical conduction through nearby molecules[6] and, conversely, transport through adjacent silicon atoms has been found to be perturbed by dipole fields due to molecules located elsewhere in the Si 7×7 cell.[7] However, no experimental work directly probing the effects of electric fields emanating from polar molecules on electrical conduction through *other* individual molecules has been reported to date. This topic is explored experimentally and theoretically in the present paper. The influence of these electric fields on electrical conduction through the underlying semiconductor substrate to which the molecules are bound is also examined. A brief account of some of the present findings has already been published.[8]

The specific systems that we study here are one-dimensional (1D) organic heterostructures consisting of chains of substituted styrene molecules grown on hydrogen-terminated Si substrates by the self-directed growth mechanism described by Lopinski and co-workers[9] originally for styrene on H:Si(100) 2×1 but subsequently applied to a wide range of molecules. The substituents in the present work are CF_3 and OCH_3 groups, one of which replaces a single hydrogen atom bound to the aromatic carbon ring of each styrene molecule. In each case the substituent is in the "para" position. Each heterostructure consists of a line of surface bound OCH_3-styrene molecules joined end-to-end (at the heterojunction) to a line of CF_3-styrene molecules. The OCH_3 group donates electrons to the aromatic ring of the styrene and is therefore positively charged while the CF_3 group withdraws electrons and is negatively charged. However, electric polarization also occurs *within* the CF_3 and OCH_3 groups themselves and we find the resulting molecular multipole fields to also play an important role in electrical conduction in these systems.

In the experimental work presented here electrical conduction between the silicon substrate and a tungsten scanning tunneling microscope (STM) tip via the molecular heterostructures was measured at room temperature in ultrahigh vacuum under a variety of bias conditions. Strongly enhanced conduction was observed through a group of several OCH_3-styrene molecules near the heterojunction at low and moderate negative substrate bias. Under positive substrate bias similar pronounced enhancement of the molecular conduction near CF_3-styrene/OCH_3-styrene heterojunctions was absent. In related heterostructures, CF_3-styrene lines in a *side-by-side* configuration were found to locally depress transport originating from filled states in the underlying silicon. As will be explained below these qualitative differences can be understood as arising from the different structural,

 ©2009 The American Physical Society

electronic, and electrostatic properties of OCH_3-styrene and CF_3-styrene molecules on silicon.

The CF_3-styrene/OCH_3-styrene heterowires were modeled theoretically by determining their ground-state electrostatic potential profiles (at zero applied bias) by means of *ab initio* density-functional-theory-based computations, and then employing semiempirical tight-binding models together with the *ab initio* electrostatic profiles, solution of the Lippmann-Schwinger equation and Landauer theory to calculate the electric current between the tungsten STM tip and the silicon substrate under bias via the molecular heterostructure. We note that while the use of density-functional theory for performing *transport* calculations in molecular wires lacks a fundamental justification and is increasingly being questioned in the literature,[3,10–22] the use of density-functional theory to calculate ground-state electrostatic potentials is justified (at least in principle) by a lemma proved originally by Hohenberg and Kohn.[23] The usefulness of such density-functional-theory-based *electrostatic potential* calculations for the present system is supported also by the fact that the present theory is able to explain the experimentally observed phenomena outlined in the preceding paragraph.

The theoretical work that is presented here demonstrates that electric fields due to intramolecular charge transfer within OCH_3-styrene and CF_3-styrene molecules can (for appropriate molecular geometries) result in enhanced electrical conduction through certain molecules in chains of OCH_3-styrene and CF_3-styrene molecules on silicon, consistent with the experimental STM data: these electric fields shift the energies of the molecular HOMO and LUMO states of *like* molecules in different parts of the chain by *differing* amounts with the result that resonant conduction begins at lower bias voltages on some molecules in the chain than on others. The differences in the observed behavior under positive and negative applied bias and between the OCH_3-styrene and CF_3-styrene molecules are accounted for in terms of this electrostatically modulated resonant transport mechanism.

The present theory predicts that conduction through individual molecules in such systems can be changed by orders of magnitude by varying the conformations of (and hence the arrangement of charges in) molecules in their vicinity. This raises the possibility of molecular switches of a new type that depend for their operation not on conformational changes in the molecular wire carrying the current (as has been discussed previously[24–26]) but on conformational changes in *other* nearby molecules that result in changes in the energy-level structure of the molecular wire. An advantage of a conformational switch based on this different principle is that the molecular wire that carries the current need not be a moving part in the device. The shorter range of electrostatic fields due to molecular dipoles (and higher multipoles) than those of electric monopoles such as the charged dangling bond studied in Ref. 6 is also advantageous, making it possible in principle to achieve higher densities of molecular switches controlled by molecular dipoles in potential device applications. The greater chemical stability of a polar molecule than a charged radical is also an important advantage. Furthermore manipulating the orientations of molecular dipoles may be an attractive alternative[27] to inducing switching by charging and discharging atomic or molecular-scale constituents of the ultimate nanoscale electronic devices.

This paper is organized as follows: the experimental methodology and results are presented in Sec. II. The theoretical model is explained and justified in Sec. III. A discussion of the relevant energy-level ordering in these systems is presented in Sec. III B. The different structures that the molecules may assume when bound to silicon are described in Sec. III C. Our theoretical results for a particular conformation of a CF_3-styrene/OCH_3-styrene molecular chain on silicon are presented in Sec. IV for positive and negative substrate bias, together with some comments as to how these theoretical results may relate to the experimental data. In Sec. V we clarify the relationship between structure, electric potentials, and transport in the CF_3-styrene/OCH_3-styrene heterostructures by considering systematically other examples of possible molecular chain geometries. Theoretical results demonstrating that the current enhancement near the CF_3-styrene/OCH_3-styrene junction is specifically an electrostatic effect are reported in Sec. VI. Simulations of heterostructures that include single and triple rows of CF_3-styrene molecules and of the influence of these molecules on the electrostatic potentials in the underlying silicon and on electron transport are reported in Sec. VII. Further discussion of the relationship between the theory and experiment is presented in Sec. VIII.

II. EXPERIMENT

STM experiments were performed under vacuum on hydrogen-terminated Si (100) 2×1 surfaces. Samples were cleaved from arsenic-doped (resistivity <0.005 Ωcm) Si (100) oriented wafers, and mounted into molybdenum sample holders. Samples were loadlocked into a vacuum system (background pressure $<1\times10^{-10}$ Torr) and degassed at 700 °C for 8 h. The samples were flash annealed to 1250 °C to remove the surface oxide and reorder the crystal surfaces. During annealing, heating was temporarily suspended if the system pressure exceeded 4×10^{-10} Torr. Clean crystalline surfaces were routinely produced with defect densities below 5%.

After cool down and inspection in the STM, the silicon crystals were transferred to the preparation chamber for hydrogen termination. Molecular hydrogen was leaked into the system (1×10^{-6} Torr) and a hot tungsten filament ($\sim$1600 °C) positioned 10 cm from the silicon sample ($T=300$ °C) dissociated the molecular gas into reactive atomic hydrogen. A 13 min exposure produced samples with a quasisaturated 2×1 silicon monohydride surface.[28]

One-dimensional molecular organic heterowires were grown under vacuum using the self-directed growth mechanism reported by Lopinski and co-workers[9] for styrene on H:Si(100) 2×1. For styrene (consisting of an aromatic carbon ring bound to a vinyl group), self-directed growth results from a chain reaction between the vinyl group of the styrene and a surface dangling bond (i.e., silicon radical exposed by a missing hydrogen atom on the surface). In forming a chemical bond with the exposed silicon atom, the terminal carbon atom on the vinyl group breaks one of its double bonds to the adjacent carbon atom, leaving the unsatisfied

bonding electron on the adjacent carbon atom to abstract a hydrogen atom from an adjacent Si dimer. The newly formed dangling bond is then free to repeat the process by reacting with another styrene molecule. Multiple reactions lead to well ordered one-dimensional chains of styrene bound along a given side of a silicon dimer row.[9]

This self-directed growth mode has been observed to occur for various alkene and carbonyl containing molecules including functionalized styrenes[29–31] making the formation of heterowires a simple matter of sequentially dosing the H:silicon surface with the desired chemical precursors.[32] The fortuitous alignment of the aromatic rings in these structures makes them ideally suited for probing transport effects resulting from overlapping π and π^* states along the molecular chain axis. The introduction of a chemical discontinuity at the heterojunction provides a means of isolating and studying effects resulting from specific intermolecular interactions. Electron donating and withdrawing substituent groups are of particular interest as they modify the energy alignment and spatial distribution of π and π^* states in host aromatic molecules. These effects lead to systematic variations in reaction rates[33] and ionization potentials[34,35] in substituted aromatic compounds. Corresponding effects on single molecule transport are under current investigation.[5]

Substituent effects in STM imaging of 4-methylstyrene/styrene heterowires were reported in Ref. 37. While the substituted methyl group had a strong (bias dependent) influence on the differential molecular height and corrugation resolved on either side of the heterojunction, the imaging characteristics of the heterowires could be understood qualitatively without considering the effects of intermolecular electrostatic interactions on the electronic structure of the heterowires; features reflecting such interactions were not observed in the experimental data. The present work revisits the earlier heterowire line-growth experiments with more strongly perturbing substituent groups:[34,35] 4-methoxystyrene (OCH_3-styrene), and 4-trifluoromethylstyrene (CF_3-styrene).

H-termination of the Si(100) samples, growth, and imaging of the molecular heterostructures were carried out within the same vacuum system. Dissolved atmospheric gases were removed from the substituted styrene precursors using multiple freeze-pump-thaw cycles prior to introduction (via leak valve) into the vacuum system. Before and after line growth, samples were imaged in STM using electrochemically etched tungsten tips, cleaned by electron bombardment, and field emission. Bias-dependent STM imaging of the structures was performed in constant-current mode (tunnel current fixed at 40 pA). Surface coordinates belonging to STM images were rescaled after acquisition to yield an orthogonal inter-row (0.768 nm) to interdimer (0.384 nm) periodicity of 2:1. Feature heights in the constant-current STM images were determined in relation to observed terrace height separation on the Si(100) surface (0.136 nm). Images of CF_3-styrene/OCH_3-styrene heterowires were acquired on multiple surfaces and studied using several different tips in two separate Omicron STM1 systems.

Figure 1 shows the growth and bias-dependent STM imaging of two CF_3-styrene/OCH_3-styrene heterowires on an H:silicon sample. After imaging the unreacted H:silicon surface (not shown), the STM tip was retracted ~1 micron from the surface. CF_3-styrene was introduced into the chamber at a pressure of 1×10^{-6} Torr for ~10 s. Sample exposure was nominally 10 L (1 L=10^{-6} Torr s). The H-terminated silicon dimer rows run diagonally between the upper left and lower right-hand corners of the image frames. The elongated white (elevated) features running along the dimer

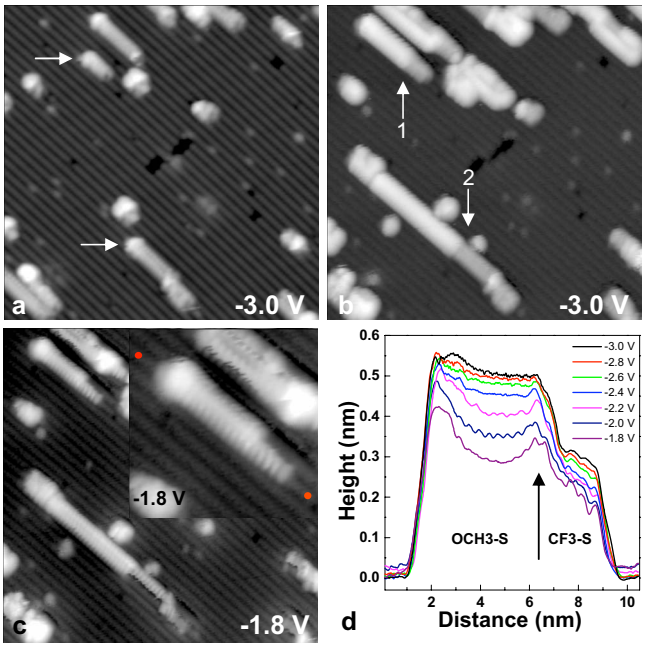

FIG. 1. (Color online) Constant-current filled-state STM images showing the growth of two CF_3-styrene/OCH_3-styrene heterowires. (a) V_s=−3.0 V. H:Si(100) surface following a 10 L exposure of CF_3-styrene. Arrows indicate positions of chemically reactive dangling bonds at the ends of the CF_3-styrene line segments. (b) Following a 10 L exposure of OCH_3-styrene, the two CF_3-styrene line segments in (a) have been extended to form two CF_3-styrene/OCH_3-styrene heterowires ("1" and "2"). At V_s=−3.0 V, the OCH_3 images higher (brighter) than the CF_3-styrene segments. (c) V_s=−1.8 V. The OCH_3-styrene near the molecular heterojunctions in heterowires 1 and 2 image with enhanced height. Molecules at the end of the OCH_3-styrene line segment in heterowire 1 also image with enhanced height in response to the terminal dangling bond. Inset: close up of heterowire 1. Molecules are bound to the right-hand side of the dimer row indicated by the red dots. (d) Constant-current topographic cross sections extracted from bias-dependent imaging of heterowire 1 along the trench to the right of the attachment dimers in (c). The height envelope for the heterostructure extends between 1 and 9.5 nm along the abscissa. The height maxima associated with the terminal dangling bond, and the molecular heterojunction are at 2.3 and 6.4 nm, respectively. At elevated bias (−3.0 V), the OCH_3-styrene images with approximately uniform height from beyond the terminal dangling bond to the heterojunction. As the bias decreases in magnitude, the OCH_3-styrene images with decreased height as the molecular π states drop below the tip Fermi level. At −1.8 V, localized height enhancement in the OCH_3-styrene due to the terminal dangling bond and also near the molecular heterojunction (black arrow) is most evident. Image areas (a)–(c): 26×26 nm^2. Inset area: 8.5×8.5 nm^2. Tunnel current: 40 pA. (a)–(d) reprinted with permission from Piva *et al.* (Ref. 8). Copyright 2008 by the American Physical Society.

rows correspond to regions where molecules have reacted with the surface. The black (depressed) features appearing most notably in the centers of Figs. 1(a) and 1(b) result from missing atoms (Si vacancies) in the silicon surface.

Figure 1(a) shows a 26×26 nm^2 region of the sample following a 10 L exposure of CF_3-styrene. Sample bias (V_s) was −3.0 V. White arrows label the reactive dangling bonds at the ends of two CF_3-styrene line segments. Due to slight tip asymmetry, CF_3-styrene bound to either side of their host dimers image with slightly different corrugation. Comparison with images of the unreacted H:silicon surface (not shown) show the upper and lower CF_3-styrene line segments are chemically bound to the right-hand and left-hand sides of their respective dimer rows.

Figure 1(b) shows the same region of the crystal (V_s=−3.0 V) following a 10 L exposure of OCH_3-styrene (1×10^{-6} Torr exposure for ~10 s). The terminal dangling bonds belonging to the upper and lower CF_3-styrene line segments in (a) have reacted with OCH_3-styrene forming two CF_3-styrene/OCH_3-styrene heterowires ("1" and "2"). At −3.0 V, the tip Fermi level is below the highest band of occupied molecular π states for the OCH_3-styrene as evidenced by the fact that at this bias voltage the experimental STM height profile of the OCH_3-styrene has saturated as can be seen in Fig. 1(d): this saturation indicates that the number of OCH_3-styrene HOMO states contributing to the STM current is no longer increasing with increasing bias so that the STM tip Fermi level must be below the highest band of OCH_3-styrene HOMO levels. However, the tip Fermi level remains above the occupied molecular π states in the CF_3-styrene at this bias because the molecular CF_3-styrene HOMO is well below the OCH_3-styrene HOMO as evidenced by gas phase molecular calculations[34] and by the present theoretical work for these molecules on silicon. This is also consistent with the CF_3-styrene molecules imaging with reduced height (less bright) in comparison to the OCH_3-styrene in Fig. 1.

Figure 1(c) shows the same region of the crystal imaged with V_s=−1.8 V. At this bias, the tip Fermi level is in the vicinity of the highest occupied molecular orbitals (π states) in the OCH_3-styrene line segment; this conclusion is based on comparisons between these experimental data and the results of our theoretical modeling as is discussed in Sec. IV B. While the OCH_3-styrene continues to image above (brighter than) the CF_3-styrene, heterowires 1 and 2 image with enhanced height (brighter) above the OCH_3-styrene molecules situated near the heterointerface. The OCH_3-styrene molecules in heterowire 1 (close up in inset) near the terminal dangling bond also image with increased height.

Figure 1(d) shows a series of 0.4 nm wide topographic cross sections extracted from heterowire 1 along the trench running between its attachment dimer row [labeled with red circles in Fig. 1(c) inset] and the vacant H-terminated dimer row to its right. Also included are curves from images (not shown) acquired at intermediate sample biases. The topographic height envelope for the heterostructure extends between 1 and 9.5 nm along the abscissa. The height maxima associated with the terminal dangling bond, and the molecular heterojunction are located at 2.3 and 6.4 nm, respectively. Postponing discussion of the interfacial height enhancement for the time being, the bias-dependent height response of the OCH_3-styrene line segment near the terminal dangling bond is much like that reported in Ref. 6 for a single homomolecular styrene line segment: at elevated negative substrate bias, ($|V_s|\gtrsim2.4$ V) the highest band of occupied π states in the OCH_3-styrene lies above the tip Fermi level and the OCH_3-styrene images with roughly uniform height. As the bias decreases in magnitude, these occupied π states of the OCH_3-styrene approach the tip Fermi level (and eventually begin to drop below it), and the molecules image with reduced height above the surface. Molecules in the vicinity of the negatively charged dangling bond on the degenerately doped n-type surface exhibit a spatially dependent reduction in ionization potential due to the electrostatic field emanating from the negatively charged dangling bond.[6,36] Thus at low bias, molecules nearest the terminal dangling-bond image with increasing height.[6]

In stark departure from the imaging characteristics of homomolecular styrene chains reported in Ref. 6, and absent from the images of the CH_3-styrene/styrene heterowires studied in Ref. 37 is the height enhancement at the heterojunction resolved at low bias. The bias-dependent height response of the OCH_3-styrene near the heterojunction is similar to that near the terminal dangling bond just described. At elevated bias, the interfacial OCH_3-styrene images with nearly constant height along the bulk of the homowire segment. As $|V_s|$ decreases, however, the height of the interfacial OCH_3-styrene (four to five molecules closest to the molecular interface) does not decay as rapidly as in the midsection of the OCH_3-styrene line segment. At the lowest filled-state bias studied for this particular heterowire, the interfacial OCH_3-styrene molecules image ~0.05 nm higher than OCH_3-styrene molecules situated five to seven dimers away from the heterojunction. The typical noise in the presented images is <0.004 nm.

Figure 2 shows filled and empty-state imaging of a cluster of three heterowires. These heterowires were identified on a region of the crystal where imaging of the H:silicon surface before line growth was not carried out. The chemical identities of the line segments were confirmed at the end of the imaging sequence by dosing with CF_3-styrene, and comparing the imaging characteristics of the newly reacted line segments (not shown) with the nearby heterowires. Characteristics in these images (in combination with those in Fig. 1) are representative of the range of tip-dependent imaging contrast encountered over the course of the experiments.

Figure 2(a) shows a filled-state constant-current STM image of the three heterowire cluster with V_s=−2.6 V. As in Fig. 1(b), the OCH_3-styrene line segments image taller (brighter) than the CF_3-styrene line segments consistent with their relative ionization potentials. In Fig. 2(b) (V_s=−2.0 V), however, the OCH_3-styrene away from the interface images lower (darker) than the CF_3-styrene. This contrast reversal (tip dependent) is often encountered at low bias in filled-state imaging. In all instances, whether or not this low bias contrast reversal occurs, height enhancement of the interfacial OCH_3-styrene remains prominent and corresponds to the height of OCH_3-styrene far from the interface at greater magnitude filled-state bias (i.e., the interfacial OCH_3-styrene images as though accompanied by a localized

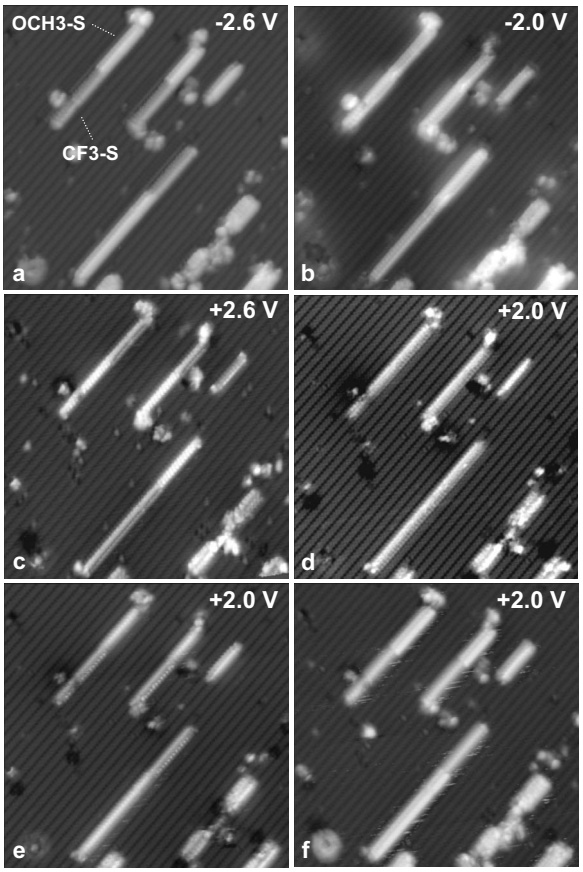

FIG. 2. [(a) and (b)] Constant-current filled-state and [(c)–(f)] empty-state STM imaging of a 3 heterowire cluster. (a) V_s=−2.6 V. OCH_3-styrene line segments image higher (brighter) than CF_3-styrene line segments. (b) V_s=−2.0 V. At low magnitude bias OCH_3-styrene can image lower than CF_3-styrene (tip dependent). Enhanced molecular conductance throughout the interfacial OCH_3-styrene remains evident. (c) V_s=+2.6 V. Consistent with the greater electron affinity of CF_3-styrene, CF_3-styrene images with increased height relative to OCH_3-styrene. (d) V_s=+2.0 V. At reduced bias, height contrast between the CF_3-styrene and OCH_3-styrene line segments decreases, and molecules image with similar corrugation. [(e) and (f)] V_s=+2.0 V. Depending on tip structure, OCH_3-styrene can image above CF_3-styrene and with varying (tip dependent) corrugation. Grayscale: black corresponds to a height of 0 nm in all images. White corresponds to heights of 0.59, 0.44, 0.28, 0.18, 0.39, and 0.18 nm in images (a)–(f), respectively. Image areas (a)–(f): 26×26 nm^2. Tunnel current: 40 pA.

increase in effective tip-sample bias magnitude).

Figures 2(c)–2(f) show empty-state images for the three heterowire cluster. In Fig. 2(c) at V_s=+2.6 V, the CF_3-styrene images above (brighter than) the OCH_3-styrene. As is discussed in Sec. IV B this result is consistent with the increased electron affinity of the CF_3-styrene (a result of the highly electronegative F atoms). As the π^* state for the CF_3-styrene is much lower than the corresponding π^* states belonging to the OCH_3 styrene, a greater number of tip states can tunnel into the CF_3-styrene (and therefore, the STM tip must travel further away from the surface above the CF_3-styrene to maintain a constant tunnel current across the heterostructure). In Fig. 2(d), V_s=+2.0 V and the tip Fermi level is presumed to lie below both the OCH_3-styrene (as before) and CF_3-styrene π^* states. The tunnel current is dominated by carrier injection into the silicon conduction band, and the molecules image (nonresonantly) with similar contrast.

Figures 2(e) and 2(f) display empty-state imaging data acquired at V_s=+2.0 V following spontaneous tip structural changes. In this imaging mode, the OCH_3-styrene images above (brighter than) the CF_3-styrene. This imaging behavior when apparent, often extends to greater bias (up to V_s=+3.2 V). In addition to this empty-state contrast reversal, changes to the molecular corrugation within the homomolecular line segments are apparent [particularly in terms of the appearance of the OCH_3-styrene between frames (d) and (f)]. It is clear in these experiments that the tip density of states plays a considerable role in determining the contrast (in terms of overall height and/or molecular corrugation) observed between the OCH_3-styrene and CF_3-styrene line segments. Tip-dependent imaging contrast in STM of organic molecules has been documented previously.[38,39]

While the empty-state imaging displays considerable contrast variation, of particular significance is the absence of notable interfacial structure. An exception to this was observed in a small portion of low bias empty-state images which revealed height enhancement for a single interfacial molecule. The height enhancement was between 0.01 to 0.02 nm, and smaller than the 0.02–0.14 nm height enhancement observed for the considerably broader (~5 molecule wide) filled-state interfacial features resolved in Figs. 1(c), 1(d), and 2(b), and others (not shown). While such a narrow empty-state feature appears in the simulation work presented in Secs. IV and V, additional observations will be required before a detailed comparison with theory can be undertaken.

Interesting behavior was also observed at low bias in filled-state imaging of heterostructures containing CF_3-styrene segments in a side-by-side configuration: Fig. 3(a) shows a 32×32 nm^2 region of the crystal imaged at V_s=−2.0 V, I_s=40 pA. While single chains of OCH_3-styrene (white) and CF_3-styrene (gray) image as protrusions with the OCH_3-styrene higher than the CF_3-styrene, regions with triple chains of CF_3-styrene (indicated by black arrows) appear as depressions.

Figures 3(b)–3(e) show the growth, and bias-dependent imaging of the (single-triple CF_3-styrene)/OCH_3-styrene heterostructure at the center of Fig. 3(a). Figure 3(b) shows the H:silicon surface following a 10 L exposure of CF_3-styrene (V_s=−3.0 V). The arrow points to the reactive dangling bond at the end of the longest CF_3-styrene line. The ⋆ marks a short double chain of CF_3-styrene that has grown beside the long CF_3-styrene chain. Figures 3(c)–3(e) show the same region following a 10 L exposure of OCH_3-styrene. The end of the long CF_3-styrene chain has been extended by approximately seven molecules of OCH_3-styrene. Figure 3(c) (V_s=+2.0 V) and Fig. 3(d) (V_s=−3.0 V) image the single and triple CF_3-styrene segments with comparable height. In Fig. 3(e), V_s has been reduced to −2.0 V and the region with the triple CF_3-styrene lines images below (darker than) the single file chain of CF_3-styrene. Figure 3(f) shows topographic cross sections along the CF_3-styrene/OCH_3-styrene heterowire. From V_s=−3 V to V_s=−2 V, the triple

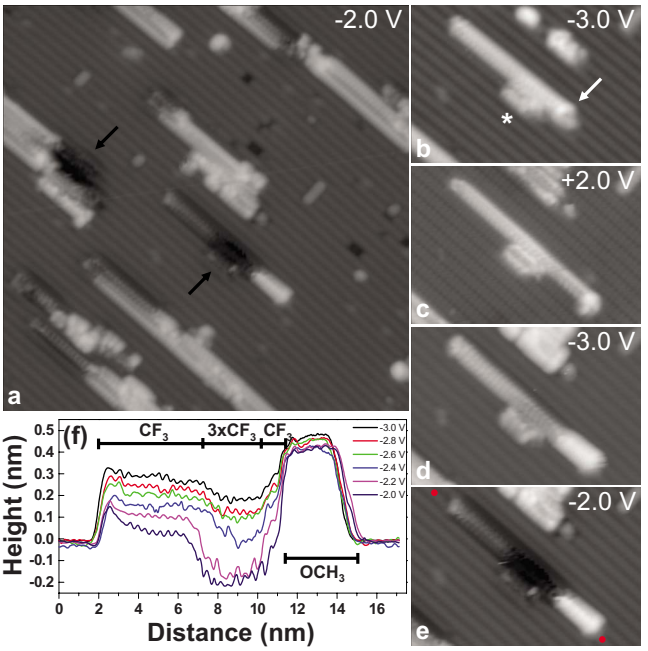

FIG. 3. (Color online) Constant-current filled-state STM images of CF_3-styrene/OCH_3-styrene heterostructures on H:Silicon. (a) $V_s=-2.0$ V. OCH_3-styrene (white) and single and double chains of CF_3-styrene (gray) image as protrusions light in appearance. Triple chains of CF_3-styrene (black arrows) appear dark. Images (b)–(e) show growth of the (single-triple CF_3-styrene)/OCH_3-styrene heterostructure at the center of (a). (b) $V_s=-3.0$ V. The white arrow indicates the position of the chemically reactive dangling bond at the end of the long CF_3-styrene segment following a 10 L exposure of CF_3-styrene. The white asterisk shows a short double CF_3-styrene line segment beside the longer single CF_3-styrene chain. (c) $V_s=+2.0$ V. Following a 10 L exposure of OCH_3-styrene, the long CF_3-styrene chain has been extended by ~7 OCH_3-styrene molecules. (d) $V_s=-3.0$ V. OCH_3-styrene appears higher (brighter) than CF_3-styrene. Single and triple CF_3-styrene segments image with similar height. (e) $V_s=-2.0$ V. Single chains of OCH_3-styrene and CF_3-styrene continue to image as bright protrusions while triple chains of CF_3-styrene do not. (f) Constant-current topographic cross sections (0.4 nm wide) extracted from bias-dependent imaging of the (single-triple CF_3-styrene)/OCH_3-styrene heterostructure along the trench to the right of the attachment dimers [indicated by red circles in (e)]. Heights are given relative to the H:silicon surface (height=0 nm). Areas (a) 32×32 nm^2; (b)–(e): 15×10 nm^2. Tunnel current: 40 pA. (b)–(f) reprinted with permission from Piva *et al.* (Ref. 8). Copyright 2008 by the American Physical Society.

CF_3-styrene chain (between 7 and 10 nm along the abscissa) images with decreasing height. Significantly, at $V_s=-2.0$ V, this region images 0.2 nm below the H:Si surface indicating depleted silicon state density beneath the molecules at the tip Fermi level.

The localized filled-state depletion effect produced by the chemisorbed CF_3-styrene was observed throughout the course of the imaging experiments. The specific filled-state bias at which the effect became visible, however, varied on the order of a volt (consistent with a change in tip electronic affinity by the same amount). Figure 4 shows an example where the localized filled-state depletion effect produced

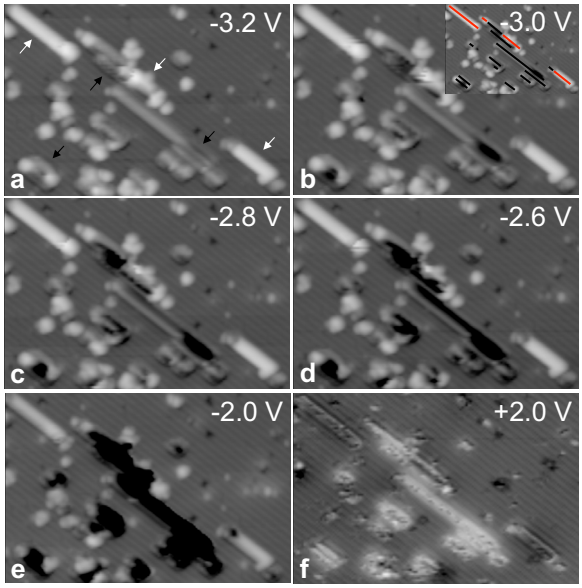

FIG. 4. (Color online) Constant-current filled-state STM imaging (a)–(e) showing the effect of overlapping CF_3-styrene lines on local surface conductance. Images show an H:Si(100) surface following exposure to 8 L of CF_3-styrene followed by 8 L of OCH_3-styrene. (a) $V_s=-3.2$ V. Both OCH_3-styrene ("white" chains indicated by white arrows) and CF_3-styrene ("gray" chains) image as protrusions. CF_3-styrene chains image with comparable height whether in isolation, or in a side-by-side configuration (indicated by black arrows). (b) $V_s=-3.0$ V. Isolated chains of CF_3-styrene image as protrusions while overlapping CF_3-styrene chains image with reduced height. Inset: $V_s=-3.0$ V. Image shows positions of CF_3-styrene chains (black lines) and OCH_3-styrene chains (red lines). (c) $V_s=-2.8$ V. At lower magnitude bias, regions with overlapping CF_3-styrene chains image with decreased height and with greater lateral extent. (d) $V_s=-2.6$ V. Single CF_3-styrene chains begin to darken in appearance and regions with overlapping CF_3-styrene chains image with greater depth. (e) $V_s=-2.0$ V. All CF_3-styrene regions image as depressions. Notably, isolated OCH_3-styrene regions appear as "bright" protrusions throughout the sequence. (f) $V_s=+2.0$ V. In empty-state imaging, both CF_3-styrene chains and OCH_3-styrene chains image as protrusions. Grayscale: (a)–(e): 0 nm (black), 0.87 nm (white), (f): 0 nm (black), 0.48 nm (white). Areas (a)–(f): 32 nm $\times$ 20 nm. Tunnel current: 40 pA.

by two overlapping CF_3-styrene lines is apparent at $V_s=-3.0$ V.

Figure 4(a) ($V_s=-3.2$ V) shows a 32×20 nm^2 surface region of H:silicon following an 8 L exposure of CF_3-styrene followed by 8 L of OCH_3-styrene. Single OCH_3-styrene chains are identified here on the basis of their increased height (0.43 nm or white) at elevated magnitude bias relative to CF_3-styrene (0.15 nm or gray) and decreased height dependence on sample bias in filled-state imaging.[40] Regions with overlapping CF_3-styrene chains (black arrows) image with similar height to single CF_3-styrene chains (extending beyond overlap regions). In Figs. 4(b) and 4(c), as $|V_s|$ is reduced CF_3-styrene chains in a side-by-side configuration image with decreasing height relative to single CF_3-styrene chains. In Fig. 4(d) ($V_s=-2.6$ V), the single CF_3-styrene chains begin to image as depressions in the H:silicon surface. In Fig. 4(e) ($V_s=-2.0$ V), all CF_3-styrene regions image as

depressions (black). The CF_3-styrene chains in a side-by-side configuration continue to image lower than the single chain CF_3-styrene regions, in this case by 0.14 nm. Throughout the filled-state imaging sequence (a)–(e), the OCH_3-styrene chains display a much smaller change in height while continuing to image as protrusions (0.43 and 0.26 nm above H:silicon at −3.2 V and −2.0 V, respectively). Figure 4(f) (V_s=+2.0 V) shows an empty-state image of the same region of the crystal. Both CF_3-styrene and OCH_3-styrene image as protrusions (bright).

Results presented in Figs. 1 and 2 and for other single chain CF_3-styrene/OCH_3-styrene heterostructures (not shown), show the presence of the chemical heterojunction causes the interfacial OCH_3-styrene to image with elevated height under low filled-state bias. The prominence (both in terms of height and lateral extent) of the filled-state interfacial feature compared with the absence of significant interfacial structure resolved in empty-state imaging in these structures, suggests an electronic origin for the effect. As the low bias imaging conditions required to observe the filled-state interfacial feature also result in decreased tip-sample separation, the possibility of tip-molecule interactions at the heterojunction leading to altered molecular conformations which contribute to the observed interfacial structure cannot be ruled out. However, such tip-induced structural changes cannot account for the differing interfacial behavior observed at low positive and negative substrate bias. The localized depletion in silicon filled-state density observed in Figs. 3 and 4 in response to the CF_3-styrene chains also cannot be understood in terms of only conformational differences between otherwise noninteracting molecules. The theoretical modeling developed in the following sections explores various factors which can account for these observations. It will be seen that conformational details in concert with electrostatics play a significant role in these phenomena.

III. MODEL

A. Formalism

In order to carry out calculations of electronic transport through molecules bonded chemically to metal or semiconductor electrodes it is necessary to know the electronic structures of these systems. *Ab initio* density-functional-calculations-based on the Kohn-Sham local-density approximation (LDA) (Ref. 41) and extensions such as generalized gradient approximations (GGA) are commonly used for this purpose. However, the theoretical foundations of this approach and the accuracy of the results that it yields for molecular *transport* calculations are increasingly being questioned in the literature at the present time:[3,10–22] while such formalisms are appropriate (at least in principle) for calculating the *total* energy, the spatial distribution of the electronic charge density and the electrostatic potential throughout inhomogeneous electronic systems in their *ground states*,[23,41] the single-electron eigenenergies and wave functions that appear in them are somewhat artificial constructs that in most cases do not have rigorous physical meanings.[3,14,19,41] Consequently, they need not be good approximations to the energies and wave functions of the true electronic quasiparticles that determine the electronic transport properties of molecular systems. Under what circumstances such *ab initio* calculations should produce acceptable results for electron transport *despite* this fundamental shortcoming, and how to obtain satisfactory results when they do not are important unresolved questions that are the subject of much ongoing research at the present time.[3,10–22,42]

For molecules adsorbed on silicon the above deficiencies of the LDA, GGA, and their relatives manifest themselves most obviously in that these approximations underestimate the band gap of silicon and yield incorrect values for the energy offset between the highest occupied molecular orbital (HOMO) of the molecule (or the relevant frontier orbital of the adsorbate) and the silicon valence-band edge. The errors in these energy offsets obtained from the density-functional calculations have recently been estimated for a few molecules to range from 0.6 to 1.4 eV.[18] Because of these and other[43] deficiencies, the predictions of transport calculations based on *ab initio* density-functional calculations of the electronic structure are unreliable for molecules on silicon; they are able to capture some observable phenomena[44] but are qualitatively incorrect for others.[18,37]

In the case of linear chains of styrene[9] and methyl-styrene[37] molecules grown by self-assembly on a hydrogenated (001) silicon surface, the incorrect offsets between the molecular HOMO levels and the silicon valence-band edge given by the density-functional calculations result in such calculations yielding qualitatively incorrect STM images for these systems.[37] In particular, at low bias the *ab initio* calculations predict *minima* in the STM height profiles of the molecular chains over the centers of the molecules where *maxima* are observed experimentally.[37] These deficiencies of the *ab initio* calculations have been overcome[37] by developing a different electronic structure model based on extended Hückel theory, a tight-binding scheme from quantum chemistry[45,46] that provides an approximate description of the electronic structures of many molecules and has also been used successfully to explain the experimental current-voltage characteristics of a variety molecular wires connecting metal electrodes[47–51] and to model the band structures of a variety of crystalline solids.[37,52,53]

Extended Hückel theory describes molecular systems in terms of a small set of Slater-type atomic orbitals $\{|\phi_i\rangle\}$, their overlaps $S_{ij}=\langle\phi_i|\phi_j\rangle$ and a Hamiltonian matrix $H_{ij}=\langle\phi_i|H|\phi_j\rangle$. The diagonal Hamiltonian elements $H_{ii}=\epsilon_i$ are taken to be the atomic-orbital ionization energies and the nondiagonal elements H_{ij} for $i\neq j$ are expressed in terms of ϵ_i, ϵ_j, S_{ij}, and phenomenological parameters chosen for consistency with experimental molecular electronic structure data. As is described in detail in Ref. 37, the standard extended Hückel theory[46] was modified so as to also provide an accurate description of the band structures of the silicon substrate and the tungsten STM tip. The energy offset between the molecular HOMO and the silicon valence-band edge (an adjustable parameter in the theory[37]) was assigned a physically reasonable value for which our transport calculations reproduced correctly the character of the height profile along the styrene and methylstyrene molecular chains observed experimentally in STM images at low bias, i.e., apparent height *maxima* over the centers of the molecules. The model proved

to be remarkably successful, accounting not only for this low bias property of the STM images, but also for several counterintuitive features of the experimental data, including the experimentally observed reversal in the contrast between the styrene and methyl-styrene molecular chains with increasing STM tip bias, the observed increase in the apparent height of the molecules at the ends of the molecular chains relative to those far from the ends with increasing bias and the observed disappearance of the corrugation of the STM height profile along the molecular chains with increasing bias.[37]

The tight-binding model based on extended Hückel theory that is described in Ref. 37 is adopted in the present work but with an important modification: a limitation of extended Hückel theory is that in it the atomic-orbital energy ϵ_i depends on the type of atom on which orbital i is located but is not influenced by the presence of other atoms in the vicinity. This is a reasonable first approximation for the styrene and methylstyrene molecules considered in Ref. 37 since those molecules do not contain strongly charged groups. However for the OCH_3-styrene and CF_3-styrene molecules that will be considered here, there is strong charge transfer between carbon atoms and fluorine and oxygen atoms that results in significant electrostatic fields that should modify the atomic-orbital energies ϵ_i of surrounding atoms. These electrostatic fields *are included* in the present model as is explained below. The resulting variation in the electrostatic potential from molecule to *like* molecule along the molecular chains has direct and striking effects on the experimental STM height profiles presented in Sec. II, as will be discussed in detail in the sections that follow.

While, as has been discussed above and in Refs. 3 and 10–22, the use of density-functional theory at the level of LDA or GGA for calculating electronic quasiparticle properties has no fundamental justification, this criticism does not apply to calculations of the ground-state electronic charge-density distribution *and the electrostatic potentials* that that have been shown by Hohenberg and Kohn[23] to be functionals of the charge density. Therefore the use of *ab initio* density-functional calculations to estimate the electrostatic contributions to the atomic-orbital energies ϵ_i that are due to charge transfer between different atoms (but are neglected in extended Hückel theory), while still involving approximations, is justified at the fundamental level. In the present work these electrostatic corrections to extended Hückel theory were included in our model in the following way:

An *ab initio* calculation was carried out[54] of the electrostatic potential W_n at the nucleus of every atom n of an atomic cluster that included a molecular chain with a total of 20 OCH_3-styrene and CF_3-styrene molecules in the geometry that they take on the silicon surface, a few layers of nearby Si atoms, and the H atoms needed to passivate the dangling bonds on the surface of this silicon cluster. A similar *ab initio* calculation was carried out[54] of the electrostatic potential U_n at the nucleus of each of these atoms in the *absence* of all of the other atoms. Thus

$$E_n = -e(W_n - U_n) \tag{1}$$

is an estimate of the contribution to the electrostatic energy of an electron in an atomic orbital on atom n that is due to the presence of all of the *other* atoms in the system, calculated self-consistently from first principles, i.e., it is the electrostatic contribution to the atomic-orbital energy that is neglected in extended Hückel theory, as discussed above. This contribution was included in the present model by making the substitution $\epsilon_i \rightarrow \epsilon_i + E_n$ (for each atomic orbital i of every atom n) in the diagonal elements $H_{ii} = \epsilon_i$ of the extended Hückel-like model Hamiltonian obtained for this system as described in Ref. 37. Because the orbital basis used is not orthogonal (as in standard extended Hückel theory), the nondiagonal matrix elements of the model Hamiltonian were also adjusted according to $H_{ij} \rightarrow H_{ij} + S_{ij}(E_n + E_m)/2$ for orbitals i and j on atoms n and m as required for gauge invariance.[55] The effect of the bias voltage applied experimentally between the STM tip and the silicon substrate on the Hamiltonian matrix H_{ij} was included in the present model as in Ref. 37.

Since in the above theoretical approach a highly compute-intensive *ab initio* calculation of the effects of charge transfer is carried out only once for any molecular chain being studied and a smaller basis set is used in the transport calculations that follow, in addition to correcting some fundamental deficiencies of density-functional theory as discussed above, the present approach is able to treat much larger systems than is practical to study by *ab initio* methods alone. This was crucial for the present work where fairly long molecular chains on Si needed to be studied and the system is not periodic along the molecular chain.

The electric current flowing between the STM tip and silicon substrate via the adsorbed molecules was evaluated as described in detail in Ref. 37 by solving the Lippmann-Schwinger equation, determining from the solution the Landauer transmission probability $T(E,V)$ that depends on the electron energy E and applied bias voltage V (Ref. 56) and evaluating the Landauer formula,

$$I(V) = \frac{2e}{h}\int_{-\infty}^{+\infty} dE\, T(E,V)[f(E,\mu_s) - f(E,\mu_d)], \tag{2}$$

where I is the current, $f(E,\mu_i) = 1/(\exp[(E-\mu_i)/kT]+1)$, and μ_i is the electrochemical potential of the source $(i=s)$ or drain $(i=d)$ electrode.[58]

The chains of OCH_3-styrene and CF_3-styrene molecules and associated silicon clusters that needed to be studied theoretically to make comparison with the experiment included too many atoms for it to be practical to determine their relaxed structures using *ab initio* density-functional theory calculations. Therefore a molecular mechanics method was adopted: chains of 40 molecules, half of the chain OCH_3-styrene and the other half CF_3-styrene, on a hydrogenated silicon cluster were relaxed using the Universal Force Field model[59] starting from a variety of initial configurations, and many different metastable relaxed structures were found. It is reasonable to suppose that many of them as well as intermediate structures between them were being sampled thermally in the experiment which was carried out at room temperature. Thus the limited accuracy of the structures given by the molecular mechanics method was deemed to be adequate for the purpose of the present study. Since the phe-

nomena of interest in the present work were observed experimentally near the junction of the OCH_3-styrene and CF_3-styrene chains, the relaxed molecular chain was truncated to a subset of 20 molecules surrounding the junction and the calculations of the electrostatic potential and of electrical conduction between the silicon substrate and STM tip via the molecules were carried out for this truncated chain of molecules and underlying H-terminated Si cluster with a dimerized (001) surface without further relaxation. The STM tip in the present work was modeled as in Ref. 37 as a 15 tungsten atom cluster with a (001) orientation and a single terminating atom, and coupled to an electron reservoir by many ideal leads.

B. Energy level ordering

In the present theoretical approach, the energy offsets between the HOMO levels of the OCH_3-styrene and CF_3-styrene parts of the molecular chain are given by the extended Hückel theory with the parameterization described in Ref. 46, modified so as to yield an accurate band structure for silicon and to include the *ab initio* electrostatic corrections E_n as discussed in Sec. III A. The same applies to the molecular LUMO levels and to the variation in the atomic-orbital energies from molecule to molecule along the molecular chain.

The molecular HOMO and LUMO levels for both types of molecules considered here reside primarily on the benzene rings of the molecules. Thus, because of the electron withdrawing (donating) nature of the CF_3 (OCH_3) group, the OCH_3-styrene HOMO is higher in energy than the CF_3-styrene HOMO,[60] and the CF_3-styrene LUMO is lower than the OCH_3-styrene LUMO. Thus the HOMO of the molecular chain as a whole is located on its OCH_3-styrene part (as has already been mentioned in Sec. II) and the LUMO of the molecular chain as a whole is located on its CF_3-styrene part.

However, as in Ref. 37, the energy offset between the molecular HOMO of the molecular chain and the silicon valence-band edge is an adjustable parameter of the present theory whose value is not known accurately: as was discussed at the beginning of Sec. III A, this offset is not given correctly by calculations based on standard density-functional theories; its accurate determination (like the determination of the energy offsets between the molecular levels and substrate Fermi levels for other molecular nanowires[1,3]) is a difficult unsolved problem of molecular electronics. However, based on the discussion of our experimental results that follows it is plausible that the molecular HOMO is located below the silicon valence-band edge and the molecular LUMO is located above the silicon conduction-band edge.

An important aspect of the experimental data presented in Sec. II is that even for the smallest values of $|V_s|$, the bias voltage between the STM tip and substrate at which imaging of the molecular chains was feasible, $|eV_s|$ was considerably larger than the band gap of silicon, for *both* positive and negative biasing of the silicon substrate relative to the STM tip. Given that the Fermi level of the STM tip at zero bias is located within the Si band gap, it therefore follows that the STM tip Fermi level was well below the top of the silicon valence band or well above the bottom of the silicon conduction band when the molecules were being imaged for negative and positive biasing of the substrate relative to the STM tip, respectively. A reasonable interpretation of this fact (that is consistent with all of the experimental data and with the results of our theoretical modeling) is that the HOMO of the molecular chain is located in energy below the silicon valence-band edge, that the LUMO of the molecular chain is above the silicon conduction-band edge, and that the experimental imaging of the molecular chains themselves (in the present study) was being carried out for STM tip Fermi energies near or above the LUMO or near or below the HOMO of the molecular chain, conditions under which enhancement of STM currents due to resonant or near resonant transport via the molecules is to be expected. This will be the view adopted in the remainder of this paper.

Thus three regimes will be considered theoretically for both positive and negative substrate bias:

(1) Very low bias at which the STM tip Fermi level lies between the Si conduction-band minimum (valence-band maximum) and the molecular LUMO (HOMO) energy levels.

(2) Low bias at which the STM tip Fermi level is slightly above (below) the lowest (highest) molecular LUMO (HOMO) level.

(3) For the lines of molecules on the silicon surface the molecular HOMO and LUMO levels are broadened into bands of energy levels because the molecules couple with each other, with the substrate and with the STM tip and also because the electrostatic potential varies along the molecular chain and thus shifts the molecular HOMO and LUMO energies of the molecules in the chain by differing amounts. In general there is more than one such molecular HOMO band and more than one molecular LUMO band present. The third regime corresponds to higher values of the bias at which the STM tip Fermi level is near the top (bottom) of the lowest (highest) molecular LUMO (HOMO) band. The widths of these bands in the present theoretical model depend on the molecular geometry but are on the order of a half of an electron volt for the HOMO case and a few tenths of an electron volt for the LUMO band.

As will be seen below, each regime is predicted to have its own characteristic signature in STM imaging that can be compared with our experimental data. These signatures do not depend qualitatively on the precise value assumed for the offset between the silicon valence-band edge and molecular HOMO level. Thus comparison between theory and experiment allows us to draw conclusions regarding the specific regimes in which the data were being taken and the physical mechanisms underlying the phenomena that were observed.

C. Prototypical geometries of the individual molecules bound to Si dimers

Different conformations have been proposed for styrene molecules on H terminated Si(100) (Refs. 9, 37, and 61) and it is reasonable to suppose that different atomic geometries are possible for the substituted styrenes on Si that are studied

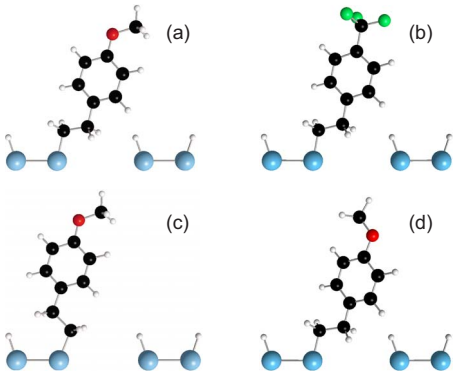

FIG. 5. (Color online) Schematic representation (Ref. 62) of some prototypical geometries of [(a), (c), and (d)] OCH_3-styrene and (b) CF_3-styrene molecules on H terminated Si(100). Si, C, O, F, and H atoms are blue, black, red, green, and white, respectively. In each case the molecule is shown together with the two Si atoms of the Si dimer to which the molecule bonds and two Si atoms of an adjacent Si dimer row. In the [(a), (b), and (d)] T-tethered geometries the molecule is located mainly over the trench between Si dimer rows while in the (c) D-tethered geometry the molecule is mainly over the Si dimer row to which it is bound. The OC bonds of the OCH_3 groups are T-oriented (toward the trench) in (a) and (c) or D-oriented (toward the dimer to which the molecule binds) in (d).

here. One possibility is that the C atom of the molecule that bonds to the C atom that bonds to the Si is located over the "trench" between two Si dimer rows as is shown in Fig. 5(a) for OCH_3-styrene and in Fig. 5(b) for CF_3-styrene. This conformation is similar to that assumed for chains of styrene molecules on Si in Refs. 9 and 37 and will be referred to as "the T-tethered geometry." In another conformation that has also been proposed for styrene on Si (Ref. 61) the C atom that bonds to the C atom that bonds to the Si is located over the Si dimer row to which the molecule bonds as in Fig. 5(c); this alternate conformation will be referred to as "the D-tethered geometry." In Figs. 5(a) and 5(c) the C atoms of the OCH_3 groups are located further over the "trench" than the O atoms are, i.e., the OCH_3 group also has the T orientation. However, the opposite (D) orientation of the OCH_3 group with the C oriented toward the Si dimer to which the molecule bonds as shown in Fig. 5(d) is also possible.

The molecular conformations described above are ideal cases: molecule-molecule interactions in the molecular chains and thermal motion at room temperature are expected to result in many intermediate geometries with the molecular benzene ring and the CO bond of the OCH_3 group not being coplanar with each other or with the silicon dimer to which the molecule bonds and the OCH_3 and CF_3 groups being rotated through different angles about the bonds that link them to their respective molecules. As will be seen below, these deviations from the ideal geometries need to be taken into consideration when modeling the experimental STM images of the molecular heterowires. However it will often be convenient in the discussions that follow to classify molecular structures according to the idealized structures such as those in Fig. 5 (T or D tethered molecule, T or D oriented OCH_3 group) that they most closely resemble.

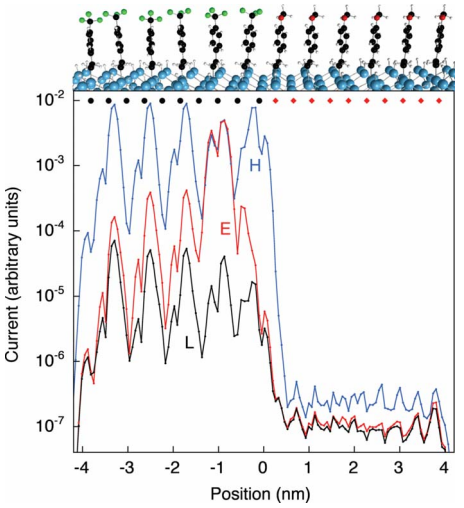

FIG. 6. (Color online) Calculated current (Ref. 63) I flowing between the tungsten STM tip and a CF_3-styrene/OCH_3-styrene molecular chain on silicon at some positive substrate biases vs STM tip position along the chain at constant tip height. A side view of a *part* of the molecular chain around the CF_3-styrene/OCH_3-styrene junction is shown at the top of the figure. Atoms are colored as in Fig. 5. A top view of the positions of some key atoms is shown in Fig. 9(a) together with the trajectory of the tungsten STM tip for the calculated current profiles. Curve L (black) is for a very low bias for which the STM tip Fermi level is between the bottom of the silicon conduction band at the Si surface and the lowest energy state derived from the molecular LUMOs. Curve E (red) is for a somewhat higher (but still low) bias for which the STM tip Fermi level is just above the lowest energy state derived from the molecular LUMOs. Curve H (blue) is for a still higher bias for which the STM tip Fermi level is near the top of the band of states derived from the molecular LUMO (Ref. 64). The STM tip Fermi level (defined relative to the molecular energy levels) differs by 0.08 eV between plots L and E and by 0.42 eV between plots E and H. Black bullets (red diamonds) at the top indicate the lateral locations of the C atoms of the molecular CF_3 groups (O atoms of the OCH_3 groups).

IV. THEORETICAL RESULTS FOR A REPRESENTATIVE MOLECULAR CHAIN GEOMETRY

A. Structure

In this section we present theoretical results for electrical conduction between the STM tip and Si substrate through a particular 20-molecule CF_3-styrene/OCH_3-styrene chain on the dimerized H-terminated (001) silicon surface. The relaxed geometry of a *part* of this molecular chain surrounding the CF_3-styrene/OCH_3-styrene junction is shown at the top of Fig. 6. Atoms are colored as in Fig. 5. Each molecule bonds to a Si atom on the same edge of the same Si dimer row (the far edge of the dimer row closest to the viewer) through a single C-Si bond as in Fig. 5. For the specific geometry shown in Fig. 6 the tethering of all of the molecules to the Si as well as the orientations of the OCH_3 groups is of the T type defined in Sec. III C. Some further details of this structure should also be noted since they shall prove to be crucial in making the connection between the theoretical results that will follow and key aspects of our experimental data: *most* of the molecules lean somewhat in

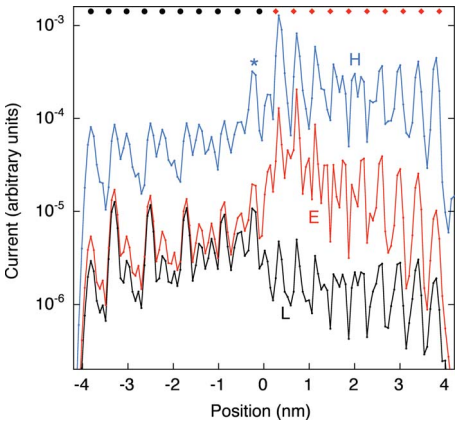

FIG. 7. (Color online) Calculated current I flowing between the tungsten STM tip and a CF_3-styrene/OCH_3-styrene molecular chain on silicon at some negative substrate biases (filled-state imaging) vs STM tip position along the chain at constant tip height. The geometry of the chain is that in Figs. 6 and 9(a) where the trajectory of the STM tip is also shown. Curve L (black) is for a very low bias for which the STM tip Fermi level is between the top of the silicon valence band at the Si surface and the highest energy state derived from the molecular HOMOs. Curve E (red) is for a somewhat higher but still low bias for which the STM tip Fermi level is just below the highest energy state derived from the molecular HOMOs. Curve H (blue) is for a still higher bias for which the STM tip Fermi level is just below the bottom of the band of states derived from the OCH_3-styrene molecular HOMO. The STM tip Fermi level (defined relative to the molecular energy levels) differs by 0.23 eV between plots L and E and by 0.52 eV between plots E and H. The black bullets (red diamonds) at the top of the plot indicate the lateral locations of the carbon atoms of the molecular CF_3 groups (O atoms of the OCH_3 groups).

the direction away from the heterojunction and also have swung outward somewhat (away from the heterojunction) about the axes of the tethering Si-C bonds, as one might expect for molecules subject to a net weak mutual steric repulsion. Due to the repulsion between the F atoms on different CF_3-styrene molecules, the CF_3 groups are all rotated through different angles about the bonds between the CF_3 groups and the molecules' benzene rings, and the benzene rings themselves are tilted somewhat differently from molecule to molecule. Because of this the detailed structure of CF_3-styrene chain is more complex and less well ordered than that of the OCH_3-styrene chain.

B. Theoretical current profiles at positive and negative substrate bias

Figure 6 shows representative results for the calculated current I flowing between the tungsten STM tip and silicon substrate via the CF_3-styrene/OCH_3-styrene chain described in the preceding paragraph at some positive substrate biases (i.e., for empty molecular state imaging) vs STM tip position along the chain at constant tip height. The corresponding results for negative substrate bias (filled molecular state imaging) are shown in Fig. 7. The black bullets (red diamonds) at the top of each plot indicate the lateral locations of the

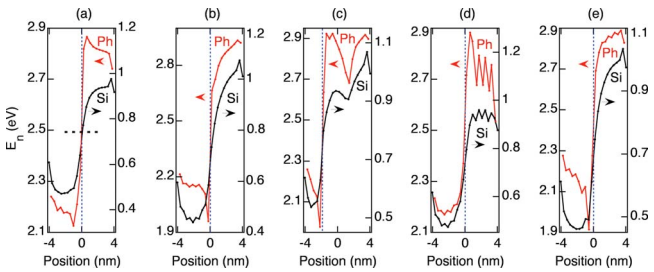

FIG. 8. (Color online) Calculated electrostatic shifts of atomic-orbital energies E_n defined by Eq. (1) vs lateral position of the orbital along the molecular chain for various molecular chain geometries. Red curves (Ph) show the average of E_n over the six carbon atoms of the benzene ring of each molecule (scale on the left axis), black curves labeled Si (right axis) show E_n for the Si atoms to which the molecules bond. Blue vertical dashed lines separate the CF_3-styrene part of the chain on the left from the OCH_3-styrene on the right. Case (a) is for the molecular chain geometry discussed in Sec. IV; the calculated current profiles for this geometry are shown in Figs. 6 and 7. The horizontal black dotted line in (a) indicates E_n for surface Si atoms if the molecules are replaced by H atoms. The distinguishing structural features of the molecular chains with the electrostatic profiles shown in panels (a)–(e) are presented in Figs. 9(a)–9(e), respectively.

carbon atoms of the molecular CF_3 groups (O atoms of the OCH_3 groups).

In both figures, curves L (black) are calculated current profiles along the molecular chain in the very low bias regime 1 introduced in Sec. III B: here the STM tip Fermi level lies between the silicon conduction-band edge and the lowest state of the molecular LUMO band in Fig. 6, and between the silicon valence-band edge and the highest state of the molecular HOMO band in Fig. 7. The red curves E are in the low bias regime 2 of Sec. III B where the STM tip Fermi level is slightly above (below) the lowest (highest) molecular LUMO (HOMO) level in Fig. 6 (Fig. 7). The blue curves H are in the higher bias regime 3 in which the STM tip Fermi level is near the top of the lowest molecular LUMO band in Fig. 6 and just below the bottom of the highest molecular HOMO band in Fig. 7.

The main features of the current plots in Figs. 6 and 7 can be understood qualitatively by considering the profiles along the molecular chain of the calculated electrostatic shifts E_n of the atomic-orbital energies defined by Eq. (1) that enter into the present model as discussed in Sec. III A. The relevant information is summarized in Fig. 8(a). There the red curve (Ph) shows the average of E_n over the six carbon atoms of the benzene ring of each molecule (the scale is on the left axis) vs the lateral position of the center of the ring along the molecular chain. Since the HOMO and LUMO of both the CF_3-styrene and OCH_3-styrene are located principally on the benzene ring, the red curve is an approximate guide as to how the molecular HOMO and LUMO orbital energies are affected by the electrostatic potentials due to charge transfer between the atoms of this system. The blue dotted vertical line separates the OCH_3-styrene part of the chain on the right from the CF_3-styrene part on the left. The black curve labeled Si (for which the scale is on the right axis) shows E_n for the Si atoms to which the molecules bond.

These electrostatic shifts differ by several tenths of an eV between the OCH_3-styrene and the CF_3-styrene parts of the molecular chain due to the different signs and magnitudes of the charge transfer between the CF_3 and OCH_3 substituent groups and the benzene rings of the respective molecules. They result in a further lowering of the HOMO and LUMO of the CF_3-styrene relative to those of the OCH_3-styrene in addition to that predicted by extended Hückel theory and also a *very local* band bending of the silicon conduction and valence bands in the immediate vicinity of the molecular chain; the Si band edges are lower in energy near the CF_3-styrene chain than near the the OCH_3-styrene. The horizontal dotted line in Fig. 8(a) indicates E_n for surface Si atoms if all molecules are replaced by H atoms bound to the Si; the effect of such (passivating) H atoms on the orbital energies of the surface Si atoms is intermediate between those of OCH_3-styrene and CF_3-styrene molecules bound to the silicon.

Because of the form of these electrostatic profiles, when the Si substrate is biased positively relative to the STM tip, the Fermi level of the metal tip crosses the Si conduction-band edge near the CF_3-styrene chain and the LUMO levels of the CF_3-styrene before doing so at the OCH_3-styrene. Thus the CF_3-styrene appears higher than the OCH_3-styrene for positive substrate bias. This is seen in the theoretical current plots in Fig. 6 and also experimentally in Fig. 2(c) although, as was discussed in Sec. II the contrast between the OCH_3-styrene and CF_3-styrene depends on the unknown microscopic details of the STM tip. As will be discussed in Sec. V it also depends on the specific conformation of the molecular chain.

The red curve (Ph) in Fig. 8(a) has a sharp minimum at the third CF_3-styrene molecule from the junction with the OCH_3-styrene chain. Thus the molecular LUMO level is lowest at that molecule. Therefore as the (positive) substrate bias increases, the Fermi level of the STM tip first crosses a molecular LUMO-derived state in the vicinity of that molecule. The prominent peak centered at the third CF_3-styrene molecule in the red current profile E in Fig. 6 thus corresponds to the onset of electron injection from the STM tip into the molecular LUMO band. There is no such feature at this molecule in the black curve L in Fig. 6 (which is at lower bias) because in that case the STM tip Fermi level is still too far away from the molecular LUMO levels for resonant tunneling through those levels to be important; thus the larger electrostatic shift of the third CF_3-styrene molecule's LUMO level does not play a large role here. When the bias is large enough for the STM tip's Fermi level to have risen to the top of the molecular CF_3-styrene LUMO band *all* of the molecular LUMO orbitals throughout the CF_3-styrene chain are transmitting resonantly so that the difference between the third CF_3-styrene molecule and the other CF_3-styrene molecules has been largely erased in the blue curve H in Fig. 6.

Notice that although the Si band edge is lowered locally around the CF_3-styrene molecules [see the black curve in Fig. 8(a)] so that one may expect the Si to appear higher in that vicinity than elsewhere in empty-state STM images, the black curve labeled Si in Fig. 8(a) does *not* show a minimum at the third CF_3-styrene molecule from the junction, confirming that it is the local electrostatic lowering of the molecular LUMO at that molecule and not the effect of the electric fields at the Si that is responsible for the prominent feature at the third CF_3-styrene molecule in the red profile E in Fig. 6.

At the bias voltages considered in Fig. 6 the tip Fermi level is well below the OCH_3-styrene LUMO states so that resonant transport via the OCH_3-styrene LUMO states is not important and thus there is little contrast between different parts of the OCH_3-styrene chain except possibly at the highest bias value shown for the OCH_3-styrene molecule that is closest to the CF_3-styrene chain.

Notice also that in Fig. 6 the contrast between the CF_3-styrene and OCH_3-styrene chains decreases markedly with *decreasing* magnitude of the applied bias. This is because the role of resonant transmission via the molecular levels in the CF_3-styrene part of the chain is decreasing rapidly whereas no resonant transmission is involved in conduction via the OCH_3-styrene which is therefore less sensitive to the magnitude of the applied bias. This behavior is in qualitative agreement with the experimental data in Figs. 2(c) and 2(d).

The qualitative features of the theoretical current profiles for negative substrate bias in Fig. 7 can also be understood by considering the electrostatic energy profiles in Fig. 8(a).

The current profile at very low bias (black curve L, Fig. 7) shows only weak contrast between different parts of the CF_3-styrene chain and between different parts of the OCH_3-styrene chain because the tip Fermi level is between the silicon valence-band edge and the molecular HOMO levels so that resonant tunneling via the molecular HOMO levels [that is strongly modulated by local extrema of the electrostatic potential along the chain of molecular benzene rings exhibited by the red curve in Fig. 8(a)] is not occurring.[65]

When the tip Fermi level falls below the highest molecular HOMO-derived level (which is located at and around the second OCH_3-styrene molecule from the junction where the electronic electrostatic potential energy [the red curve B in Fig. 8(a)] has its maximum) the current develops a strong maximum there because of the onset of resonant conduction via the molecular HOMO in that vicinity. This is why the red curve E of Fig. 7 has a strong maximum at the second OCH_3-styrene molecule from the junction.

With further increase in the bias voltage the tip Fermi level moves deeper into the molecular HOMO band and resonant transport via molecular states derived from the molecular HOMO becomes possible in other parts of the OCH_3-styrene chain as well and thus the peak in the current profile of the OCH_3-styrene chain becomes less pronounced, as in the blue curve H in Fig. 7. Notice also that with increasing bias the boundary between the OCH_3-styrene and CF_3-styrene chains becomes blurred with the higher current typical of the OCH_3-styrene chain extending to the nearest one or two CF_3-styrene molecules, as in the feature labeled * in the blue curve H in Fig. 7.

Another feature of Fig. 7 is the reversal in the contrast between the OCH_3-styrene and CF_3-styrene chains between low and intermediate bias: curve L is higher for the CF_3-styrene while curves E and H are higher for the OCH_3-styrene. This is possible because the transport mechanisms for the OCH_3-styrene in the low and intermediate bias regimes are different: the latter is dominated by resonant

conduction via the molecular HOMO levels while the former is not. Whether such a contrast reversal with increasing bias occurs or not was found in the present theoretical study to depend on the structures of the molecular chains: for the geometry shown at the top of Fig. 6 (see also Fig. 5) the OCH_3 groups lie especially low relative to the CF_3 groups which makes it possible for the CF_3-styrene molecules to appear higher than the OCH_3-styrene at low negative substrate bias. This occurs despite the fact that both the molecular HOMO levels and the local Si valence-band edge are higher in energy on the OCH_3-styrene side of the heterowire. For some other geometries of the CF_3-styrene/OCH_3-styrene chain to be discussed in Sec. V the OCH_3 groups lie higher relative to the CF_3 groups and no contrast reversal is found theoretically: the OCH_3-styrene appears higher than the CF_3-styrene even at low negative substrate bias. In experiment, contrast reversal between the OCH_3-styrene and CF_3-styrene chains with changing bias was observed in some runs (as in Fig. 2) but not in others (as in Fig. 1), most likely due to undetermined differences between the STM tips involved.

A significant difference between the calculated current profiles in Figs. 6 and 7 and our experimental STM height profiles is that the latter do not show the quasiperiodic modulation with a period of roughly two molecular spacings seen in the calculated current profiles for the CF_3-styrene part of the chain. This difference can be understood as follows: this quasiperiodic modulation of the calculated CF_3-styrene chain current profile is a geometrical effect due to the differing orientations of the CF_3 groups and also the associated differing tilts of the molecules along the CF_3-styrene chain described near the end of Sec. IV A. Therefore it is reasonable to expect this modulation not to be visible in STM images taken at room temperature where the CF_3 groups are rotating rapidly about their axes and the local phase of the spatial current modulation is therefore fluctuating rapidly so that only an average over many structures with different phases is observed on the time scale on which the STM scans are recorded, and thus a period equal to the molecular spacing is observed.

C. Current peaks near the CF_3-styrene/OCH_3-styrene interface

The prominent peaks in the red current profiles E in Figs. 6 and 7 near the interface between the CF_3-styrene and OCH_3-styrene molecular chains have the following important characteristics: the peak for positive substrate bias in Fig. 6 is narrow, just one molecule wide and occurs on the CF_3-styrene side of the junction. The peak at negative substrate bias in Fig. 7 is broader, extending over a few molecules and occurs on the OCH_3-styrene side of the junction. These properties of the interfacial peak at negative substrate bias are consistent with the experimental data presented in Sec. II. Furthermore the interfacial peak at negative substrate bias was seen experimentally at low bias in all of the many CF_3-styrene/OCH_3-styrene heterojunctions that we imaged and persisted when the STM tip changed spontaneously in the course of the imaging. By contrast, in empty-state imaging (i.e., for positive substrate bias), no discernible height enhancement at the interface was usually observed.

The above discussion in Sec. IV B identified the interfacial peaks in the calculated current profiles as being due to a maximum or minimum of the electrostatic contribution to the molecular HOMO or LUMO energy along the molecular chain occurring at the location of the peak. However, in order to understand the physics underlying the differences between the predicted properties of the peaks at positive and negative substrate bias and the similarities and differences between the predictions and experiment it is necessary to examine how these features of the current profiles depend on the structure of the molecular chain. This will be explored in the next section.

V. RELATIONSHIP BETWEEN STRUCTURE, ELECTROSTATICS AND CURRENT PROFILES

Several significant aspects of the structures of the experimentally realized molecular chains such as whether the molecules are tethered to the Si in the T or D orientation (as defined in Sec. III C) and whether the OCH_3 groups are T or D oriented, are not obvious from a direct inspection of the experimental STM images. It is also not clear theoretically which types of these structures should be favored by the kinetics of the growth process or by energetics at room temperature. Thus it is desirable to study a variety of plausible relaxed molecular chain geometries theoretically and to clarify how their structures relate to their electrostatic and current profiles. This is done in the present section and the results presented here also elucidate the mechanisms underlying the phenomena described in Secs. II and IV. Potential-energy profiles were calculated for many relaxed chain geometries and a few representative examples will be discussed below, along with possible experimental implications.

A. Notation

The important features of these molecular chain geometries are summarized in Fig. 9 where projections of the positions of some key atoms of the molecular chains onto the Si (001) plane are shown: each panel in Fig. 9 shows two rows of Si surface atoms belonging to *different* Si dimer rows. In each case the molecules are tethered to the lower row of Si atoms. The C atoms that bond to the Si atoms are orange. The C atoms that bond to the C atoms that bond to the Si atoms are violet. The C atoms of the CF_3 and OCH_3 groups are black. The O atoms are red and the F atoms are green. The C atoms belonging to the benzene rings that bond to O atoms or to C atoms not belonging to the benzene rings are white. The other C atoms of the benzene rings, the H atoms and the other Si atoms are not shown for clarity. The dashed line shows the path of the tip atom of the STM for the theoretical STM current profiles for each structure that are presented in this paper.

The structure considered in Sec. IV will henceforth be referred to as "Structure (a)" as per its label in Fig. 9. The other structures to be discussed here will be referred to similarly, according to their labeling in Fig. 9. Each of these

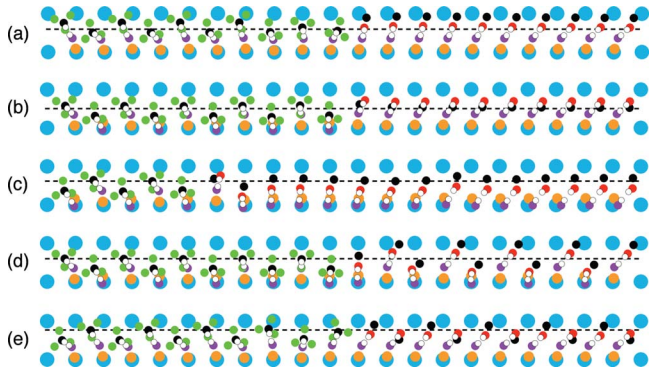

FIG. 9. (Color online) Atomic positions projected onto the Si(001) surface for some CF_3-styrene/OCH_3-styrene molecular chains on silicon studied theoretically in this work. Each panel shows two rows of Si atoms belonging to *different* Si dimer rows. The molecules are tethered to the lower row of Si atoms in each panel. The C atoms that bond to the Si atoms are orange. The C atoms that bond to the C atoms that bond to the Si atoms are violet. The C atoms of the CF_3 and OCH_3 groups are black. The O atoms are red and the F atoms are green. The C atoms belonging to the benzene rings that bond to O atoms or to C atoms not belonging to the benzene rings are white. The other C atoms of the benzene rings, the H atoms and the other Si atoms are not shown for clarity. The dashed lines show the paths of the apex atom of the STM tip for the theoretical STM current profiles presented in this paper. (a) is the structure for Figs. 6 and 7. (b)–(e) correspond to Figs. 10–13, respectively. The STM tip heights above the top layer of silicon for the calculated current profiles presented in this paper for geometries (a)–(e) are 1.161, 1.246, 1.231, 1.241, and 1.231 nm, respectively.

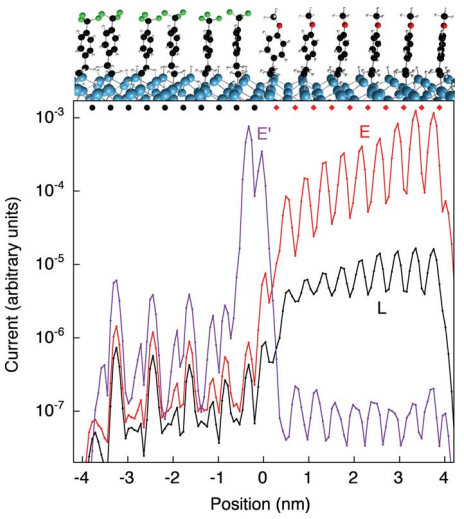

FIG. 10. (Color online) Calculated current I flowing between the tungsten STM tip and a CF_3-styrene/OCH_3-styrene molecular chain on silicon vs STM tip position along the chain at constant tip height for the molecular geometry shown at the top of the figure and in Fig. 9(b) where the trajectory of the STM tip is also shown. Notation as in Fig. 6. Curve L (black) is for a very low negative substrate bias for which the STM tip Fermi level is between the top of the silicon valence band at the Si surface and the highest energy state derived from the molecular HOMOs. Curve E (red) is for a somewhat higher but still low negative substrate bias for which the STM tip Fermi level is just below the highest energy state derived from the molecular HOMOs. The STM tip Fermi level (defined relative to the molecular energy levels) differs by 0.4 eV between plots L and E. Curve E′ (violet) is for a low positive substrate bias for which the STM tip Fermi level is just above the lowest state derived from the molecular LUMO.

structures consists of 20 molecules taken from the central region of a relaxed 40 molecule chain without further relaxation, as described at the end of Sec. III A.

B. Structure (b)

In Structure (b), as in Structure (a), the OCH_3-styrene molecules are tethered to the Si in the T orientation. But the OCH_3 groups are approximately reversed relative to Structure (a) and are now in the D orientation (defined in Sec. III C). In Structure (b) the tethering of the CF_3-styrene molecules to the Si alternates between T and D and the orientation of the F atoms in the CF_3 groups also alternates from molecule to molecule. However since this is a relaxed structure neither the OCH_3-styrene chain nor the CF_3-styrene chain has a truly periodic geometry.

1. Electrostatic and current profiles

The electrostatic potential-energy profiles along the chain of benzene rings and along the row of Si atoms to which the molecules of Structure (b) bond are the red and black curves in Fig. 8(b), respectively. Some representative current profiles for Structure (b) calculated at constant tip height along the dashed line in Fig. 9(b) are shown in Fig. 10 together with a side view of a part of this molecular chain. The qualitative behavior of the calculated current profiles in Fig. 10 can be understood by considering the features of the potential-energy profile along the chain of benzene rings in Fig. 8(b) and applying reasoning analogous to that in Sec. IV B: the current profile under a moderately low positive substrate bias for which the STM tip Fermi level is just above the lowest level of the molecular LUMO band (the violet curve E′) has a strong maximum one molecule wide at the CF_3-styrene molecule next to the OCH_3-styrene chain where the benzene ring potential-energy profile has its sharp minimum. The current profile under a moderately low negative substrate bias for which the STM tip Fermi level is just below the highest level of the molecular HOMO band (the red curve E) rises gradually to a broad maximum at the end of the OCH_3-styrene chain *remote from* the CF_3-styrene where the benzene ring potential-energy profile has its broad maximum. Unlike in Fig. 7, in this case there is no contrast reversal between the OCH_3-styrene and CF_3-styrene chains with increasing negative substrate bias; the OCH_3-styrene is higher in both the very low bias profile L and the moderately low bias profile E. This is because the OCH_3 group is located higher relative to the CF_3 group in Structure (b) than in Structure (a).

2. Significance of the results

The two main differences between the electrostatic profiles for Structure (b) and those for Structure (a) [shown in Figs. 8(a) and 8(b)] are:

(1) The minimum of the benzene ring electronic potential-energy profile (while remaining very sharp) has shifted from the third CF_3-styrene molecule from the heterojunction in Fig. 8(a) to the CF_3-styrene molecule next to the heterojunction in Fig. 8(b).

(2) The maximum of the benzene ring potential-energy profile while remaining broad has shifted from the vicinity of the heterojunction (on the OCH_3-styrene side) in Fig. 8(a) to the vicinity of the end of the OCH_3-styrene chain that is remote from the heterojunction in Fig. 8(b).

Systematic studies of various structures and their potential-energy profiles showed the reversal of the slope of the potential-energy profile along most the chain of benzene rings of the OCH_3-styrene chain from Structure (a) to Structure (b) in Fig. 8 should be attributed *not* to the OCH_3 groups being switched from the T to the D orientation per se, but primarily to the fact that the *projection onto the axis of the molecular chain* of the dipole moment associated *internal* charge structures of the OCH_3 groups (negative O and positive CH_3) has reversed direction from Structure (a) to Structure (b) as is evident from the geometries of the two structures in Fig. 9. This reversal of the charge structure along the molecular axis should lead to a reversal of the slope of the potential-energy profile and this is what is in fact seen in Fig. 8.

In this way the change in the geometrical structure of the OCH_3-styrene chain has resulted in the shift of the potential-energy maximum (and STM tip current maximum at moderately low negative substrate bias) from the vicinity of the heterojunction to the vicinity of the far end of the OCH_3-styrene chain.

An important point to note is that because of the geometrical structure of the OCH_3-styrene molecules and the way in which they bond to the silicon the internal dipole moment of the OCH_3 group has a strong component *parallel* to the silicon surface and the OCH_3 groups of all of the OCH_3-styrene molecules can be aligned in such a way that the projections of the OCH_3 groups of *all* of these molecules onto the axis of the molecular chain have the same sign. This results in a gradual buildup of the electrostatic potential along the OCH_3-styrene chain and a *broad* electrostatic potential-energy peak near one of its ends as in Fig. 8(a) or 8(b), and consequently a broad current peak under moderately low negative substrate bias, consistent with the experimental results presented in Sec. II.

By contrast, because the geometrical orientation of the CF_3 group (see Fig. 5) and the arrangement of charges within it are different than for the OCH_3 group, and because of the repulsion between the F atoms on different molecules (see the end of Sec. IV A), such a well ordered arrangement of dipole projections onto the axis of the molecular chain does not occur for the CF_3-styrene chain. Thus the electrostatic potential-energy minimum on the CF_3-styrene side of the heterojunction is a much more local phenomenon. Its location is determined by the orientations of a few molecules surrounding it and by the fringing electrostatic field of the OCH_3-styrene chain that extends across the heterojunction into the CF_3-styrene chain. Thus the electrostatic potential-energy minimum on the CF_3-styrene side of the heterojunction is very narrow and its location is sensitive to the details of the local molecular geometry. It is therefore reasonable to expect any profile peak associated with it in STM imaging at room temperature (at positive substrate bias), if present at all, to be more strongly impacted by thermal fluctuations in the molecular geometry and therefore less readily observed than the corresponding peak at negative substrate bias on the OCH_3-styrene side of the molecular chain. This is consistent with the differences between the experimental results obtained under positive and negative substrate bias that are presented in Sec. II.

Experimentally, height enhancement was observed in the STM images toward the end of the OCH_3-styrene chain that is far from the junction with the CF_3-styrene at low negative substrate bias as can be seen, for example, in Fig. 1(d). Because in this work the growth of the OCH_3-styrene chain followed the growth of the CF_3-styrene, a charged dangling bond is normally expected to be present at the end of the OCH_3-styrene chain (remote from the CF_3-styrene/OCH_3-styrene junction) where the growth of the molecular chain terminated, as in previous experimental work on styrene chains on silicon.[6,9] The electrostatic potential due to this charged dangling bond gives rise to enhancement of the height profile of the molecular chain in its vicinity in STM experiments as is discussed in Ref. 6. If alignment of OCH_3-styrene molecular dipoles as in Structure (b) was occurring in the present experiments, the associated electrostatic profiles such as in Fig. 8(b) would *also* contribute to enhanced current near the end of the molecular chain as in curve E in Fig. 10, and hence to the enhanced height profile there in constant-current STM experiments as in Fig. 1(d). Determining experimentally whether such a molecular dipole contribution to the height profile in vicinity of the dangling bond is present or not is in principle possible by passivating the dangling bond through the addition of a H atom and observing whether any height enhancement remains afterward near the end of OCH_3-styrene chain. Carrying out such a test was beyond the scope of the present experimental work. However, the fact that height enhancement was *consistently* observed experimentally near the CF_3-styrene/OCH_3-styrene heterojunction at low negative substrate bias suggests that OCH_3-styrene chains with dipole fields similar to that arising from Structure (a) rather than Structure (b) in Fig. 8 played the dominant role in these experiments.

C. Structure (c)

Structure (c) consists of 5 CF_3-styrene and 15 OCH_3-styrene molecules. The geometry of the CF_3-styrene molecules and of the OCH_3-styrene molecule that is next to the CF_3-styrene is similar to that of the corresponding molecules in Structure (b). However, as can be seen in Fig. 9(c), the other OCH_3-styrene molecules in Structure (c) have a different geometry: they are tethered to the Si in the D orientation and their OCH_3 groups are in the T orientation. Between the eighth and ninth OCH_3-styrene the molecules from the junction with the CF_3-styrene there is another abrupt change in the molecular geometry: although the molecules to the right and left of this dislocation are both D-tethered and the OCH_3's are T oriented, the molecules to the right of the fault

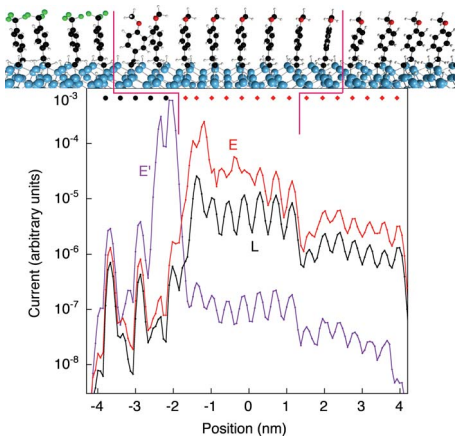

FIG. 11. (Color online) Calculated current *I* flowing between the tungsten STM tip and a CF_3-styrene/OCH_3-styrene molecular chain on silicon vs STM tip position along the chain at constant tip height for the molecular geometry shown at the top of the figure and in Fig. 9(c) where the trajectory of the STM tip is also shown. The magenta lines mark the locations of the CF_3-styrene/OCH_3-styrene interface (left) and of the dislocation in the OCH_3-styrene chain (right) in the image at the top of the figure and in the current plots below. Notation as in Fig. 5: Curve L (black) is for a very low negative substrate bias for which the STM tip Fermi level is between the top of the silicon valence band at the Si surface and the highest energy state derived from the molecular HOMOs. Curve E (red) is for a higher but still low negative substrate bias for which the STM tip Fermi level is just below the highest energy state derived from the molecular HOMOs. The STM tip Fermi level (defined relative to the molecular energy levels) differs by 0.4 eV between plots L and E. Curve E′ (violet) is for a positive substrate bias for which the STM tip Fermi level is just above the lowest state derived from the molecular LUMOs.

tilt more to the right and their OCH_3 groups are oriented nearly perpendicularly to the axis of the molecular chain.

This is reflected in the electrostatic potential-energy profile along the chain that is plotted in Fig. 8(c): since the molecular structure at the junction is similar to that for Structure (b) the potential profile on the benzene rings is also similar there, i.e., there is a sharp potential-energy minimum at the CF_3-styrene molecule at the junction. Since for OCH_3-styrene molecules 2–8 from the junction the orientation of the O and two C atoms bonded to it is similar to that for the OCH_3-styrene molecules in Structure (a) the orientation of the relevant dipoles on that part of the chain is also similar and thus the potential-energy profile is also qualitatively similar: there is a broad potential-energy maximum on the OCH_3-styrene benzene rings peaked near the junction with the CF_3-styrene. However, the different orientation of the charged groups of the ninth–fifteenth OCH_3-styrene molecules from the junction results in a reversal of the slope of the potential profile and the electronic potential energy on the OCH_3-styrene benzene rings rises to another maximum near the right-hand end of the molecular chain.

The calculated STM current profiles for Structure (c) shown in Fig. 11 are again consistent with the potential-energy profile along the chain of benzene rings: at moderately low positive substrate bias (violet curve E′) the current profile has a sharp maximum one molecule wide at the CF_3-styrene molecule where the potential-energy minimum along the molecular chain is located. At moderately low negative substrate bias (red curve E) there is a broad current maximum peaked on the OCH_3-styrene side of the junction where the potential energy has one of its maxima. From there the current falls off to a minimum near the middle of the OCH_3-styrene chain where the potential-energy curve also has its minimum. To the right of this minimum both the potential energy and current rise again but the current does not rise as high as near the junction and then begins to fall off again. This difference is due to the fact that for the red curve E the electron transmission through the molecules has not quite reached resonance for the OCH_3-styrene HOMOs at the right end of the OCH_3-styrene chain (although it has done this for the OCH_3-styrene near the junction) and also because the OCH_3-styrene molecules are tilted more at the right end of the chain than at the left. This geometrical difference also shows up as a step in the other current profiles in Fig. 11 at the dislocation in the OCH_3-styrene chain.

For Structure (c) there is again no reversal of the contrast between OCH_3-styrene and CF_3-styrene chains with increasing bias.

D. Structure (d)

In Structure (d) the geometry of the CF_3-styrene chain is broadly similar to those of Structures (b) and (c). However, in the OCH_3-styrene chain the tethering to the Si alternates between D and T. The orientation of the OCH_3 groups is all T and most of the relevant OC dipoles are oriented roughly as for Structure (a). Thus one should expect a potential-energy profile along the chain of OCH_3-styrene benzene rings somewhat similar to that for Structure (a). Indeed the red curve in Fig. 8(d) does have its maximum in the OCH_3-styrene chain near the junction with the CF_3-styrene and it declines overall to the right, but the decline is modulated by strong oscillations due to the different tethering of alternate OCH_3-styrene molecules to the Si. The potential-energy profile along the chain of benzene rings on the CF_3-styrene chain of Structure (d) is quite different than that for Structures (b) and (c): there is no potential-energy minimum on the CF_3-styrene next to the junction but instead a shallow minimum near the middle of the CF_3-styrene chain.

The current profiles for Structure (d) are shown in Fig. 12 for moderately low positive substrate bias (violet curve E′) and moderately low negative substrate bias (red curve E). Again the maxima of these profiles are near the lowest and highest points of the potential-energy profile along the chain of benzene rings, respectively. But in this case the potential-energy peak in the OCH_3-styrene chain is less prominent and narrower than in the previously discussed cases due to the less uniform structure of the array of dipoles. The broad potential-energy minimum in the CF_3-styrene results in a broader current peak at positive substrate bias than in the cases discussed earlier.

This illustrates further the strong sensitivity of the CF_3-styrene chain's potential minima to the precise details of the conformation of a single molecule or a few molecules: in

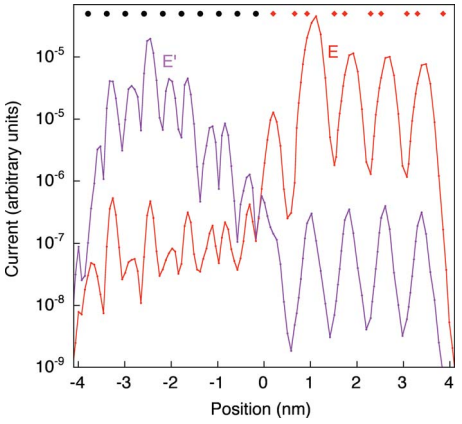

FIG. 12. (Color online) Calculated current I flowing between the tungsten STM tip and a CF_3-styrene/OCH_3-styrene molecular chain on silicon vs STM tip position along the chain at constant tip height for the molecular geometry shown in Fig. 9(d) where the trajectory of the STM tip is also shown. Curve E (red) is for a low negative substrate bias for which the STM tip Fermi level is just below the highest energy state derived from the molecular HOMOs. Curve E′ (violet) is for a positive substrate bias for which the STM tip Fermi level is just above the lowest state derived from the molecular LUMOs.

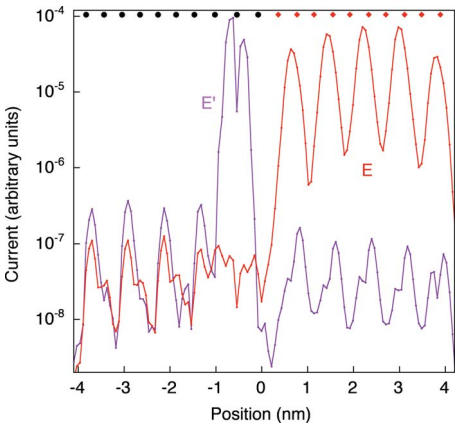

FIG. 13. (Color online) Calculated current I flowing between the tungsten STM tip and a CF_3-styrene/OCH_3-styrene molecular chain on silicon vs STM tip position along the chain at constant tip height for the molecular geometry shown in Fig. 9(e) where the trajectory of the STM tip is also shown. Curve E (red) is for a low negative substrate bias for which the STM tip Fermi level is just below the highest energy state derived from the molecular HOMOs. Curve E′ (violet) is for a positive substrate bias for which the STM tip Fermi level is just above the lowest state derived from the molecular LUMOs.

Structure (d) the OCH_3-styrene molecule at the junction of the chains is D-tethered and the OCH_3 group is T oriented while the reverse is true for Structures (b) and (c) while the CF_3 groups are rotated slightly differently and CF_3-styrene at the junction tilts somewhat differently.

E. Structure (e)

Structure (e) is similar to Structure (a) except that now the orientations of the OCH_3 groups alternate between T and D and the CF_3 groups have rotated about their axes through substantial angles. Because of the alternating orientations of the OCH_3 groups the electric fields due to the different OCH_3-styrene molecules are not aligned and produce a potential-energy profile in Fig. 8(e) with a very broad maximum near the end of the chain remote from the junction. The different orientations of the CF_3 groups than in Structure (a) result in a sharp potential-energy minimum at the second CF_3-styrene molecule from the junction.

The current profiles for Structure (e) are shown in Fig. 13 for moderately low positive substrate bias (violet curve E′) and moderately low negative substrate bias (red curve E). As expected for such a potential-energy profile we see a strong narrow current peak on the second CF_3-styrene molecule from the junction. The broad potential-energy maximum on the OCH_3-styrene chain produces a broad current maximum peaked toward the end of the OCH_3-styrene chain that is remote from the junction at intermediate negative substrate bias.

For both Structure (e) and Structure (d) the alternating geometries along the OCH_3-styrene chains result in a strong modulation of the current with a period of 2 molecular spacings. Since this modulation is not seen experimentally, either these structures are not realized in the experiments or the experiments are averaging over geometries for which the modulation occurs with different phases due to thermal fluctuations of the molecular geometries at room temperature.

VI. ELECTROSTATIC VS ELECTRONIC MOLECULE-MOLECULE COUPLING

For comparison, similar calculations to those described above were also carried out for Structure (a):

(i) *Omitting* the environmental electrostatic shifts of atomic-orbital energies E_n defined by Eq. (1). No enhancement of the current near the heterojunction (such as in curves E in Figs. 6 and 7) was found in those calculations.

(ii) Transport calculations were also carried out including the electrostatic shifts E_n but with all Hamiltonian matrix elements and basis function overlaps responsible for direct electronic hopping from molecule to molecule switched off. These calculations produced very similar current profiles along the molecular chain to those in Figs. 6 and 7, including the interface current peaks and even the feature labeled ⋆ in the blue curve H in Fig. 7. However these features appeared at somewhat different values of the bias voltages because the molecular HOMO and LUMO bands are narrower (as expected) when the intermolecule Hamiltonian matrix elements and basis state overlaps are turned off.

These results confirm that the enhanced current features near the interface in Figs. 6 and 7 result from electrostatic fields established by the polar molecules. These results therefore suggest an electrostatic origin for the filled-state interfacial enhancement resolved experimentally in Figs. 1 and 2 at low bias. (Significantly, no such interfacial current enhancement was observed experimentally[37] in styrene/methylstyrene heterostructures on Si where molecular electric fields

are expected to be much weaker because of the weaker charge transfer within those molecules.)

Furthermore, although electronic hopping from molecule to molecule may be occurring quite efficiently in substituted styrene chains on Si(100) as is discussed in Ref. 37, these calculations demonstrate the hopping not to be necessary for the occurrence of the interfacial features reported in the present work.

VII. MODELING SINGLE-TRIPLE ROW CF_3-STYRENE HETEROSTRUCTURES AND THEIR INFLUENCE ON CONDUCTION THROUGH THE UNDERLYING SILICON

The main features of the calculated current profiles of the molecular heterostructures modeled theoretically in the preceding sections derive directly from the electronic structures of the molecules themselves modulated by the electrostatic fields due to other nearby molecules. This however is not the case for the most striking feature of the experimental data shown Figs. 3(e) and 3(f) where at low negative substrate bias the electric current passing through a triple row of CF_3-styrene molecules is strongly depressed relative to that passing through the nearby single row of CF_3-styrene molecules. Our theoretical findings presented below suggest that the influence of the adsorbed CF_3-styrene molecules on the electrostatic potential *in the underlying silicon* may be responsible for this phenomenon.

Representative results of our calculations are presented in Fig. 14. The molecular geometry studied is shown schematically in Fig. 14(a). In the model considered the long CF_3-styrene line is located between the two short ones to minimize sensitivity to the Si cluster edges. All of the molecules are assumed to be tethered to the silicon in the T orientation defined in Sec. III C and shown in Fig. 5(b). Figure 14(b) shows the simulated constant height current along the long (central) CF_3-styrene line. At low negative substrate bias (for which the STM tip Fermi level is close to the silicon valence-band edge), the calculated current (curve V) drops by a factor of ~26 from the tallest current peak near the left-hand end of the single CF_3-styrene line to the tallest peak near the right-hand end of the central line of the triple CF_3-styrene structure. The origin of this effect is seen in the solid black curve labeled "Si" in Fig. 14(c): dipole fields associated with the CF_3-styrene molecules lower the Si orbital energies below the triple CF_3-styrene by ~0.2 eV more than under the single file CF_3 styrene. At low bias this reduces the silicon electronic density of states near the silicon surface at the Fermi level of the STM tip more under the triple CF_3-styrene line than under the single CF_3-styrene line, resulting in the weaker tip current through the former. As the magnitude of the bias increases eventually the tip Fermi level is lowered further by an amount substantially exceeding the differential electrostatic energy shift between the Si orbitals under the triple and single CF_3-styrene lines and thus the contrast between the STM tip currents through the triple and single CF_3-styrene lines becomes weaker as is seen in curve L of Fig. 14(b) for which the tip Fermi level is 0.5 eV lower than for curve V.

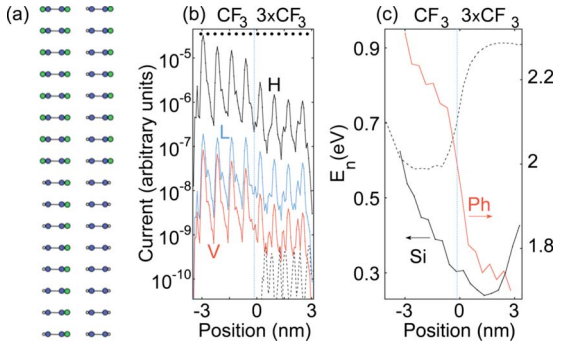

FIG. 14. (Color online) (a) Schematic top view (not to scale) of model single-triple CF_3-styrene structure. Molecules are green, surface Si atoms are blue, and H atoms are white. The single CF_3-styrene row consists of eight molecules, the triple row of 24 molecules. All molecules are T-tethered to Si; see Fig. 5(b). (b) Plots V, L, and H are calculated current profiles for an STM tip trajectory at constant height along center row of CF_3-styrene molecules in (a) for negative substrate bias. The STM tip height above the top layer of silicon is 1.261 nm. Plot V: low bias; tip Fermi level near highest Si valence-band states. Plot L: stronger bias but tip Fermi level above CF_3-styrene HOMO energies (Ref. 66). Plot H: still stronger bias; tip Fermi level well within the HOMO energy band of the *single* CF_3-styrene row but above the HOMO band of the center row of the triple CF_3-styrene. As in experiment, contrast between triple and single CF_3-styrene rows in blue profile L is much weaker than in red profile V. Dashed black curve: calculated current profile along short CF_3-styrene row on left in (a) at same tip height and bias as plot V. The STM tip Fermi level (defined relative to the molecular energy levels) differs by 0.5 eV between plots V and L and by 0.95 eV between plots L and H. Black bullets locate C atoms of CF_3 groups in the long CF_3-styrene row. (c) Black solid curve (Si): electrostatic electronic energy shifts E_n at Si atoms to which molecules of the long CF_3-styrene row bond. Triple (single) rows are right (left) of vertical dotted line. Red curve (Ph): average of E_n over the six carbon atoms of the benzene ring of each molecule of the long CF_3-styrene row (scale on right axis). Black dashed curve shows for comparison E_n at Si atoms to which molecules of a *single*-row heterostructure of ten CF_3-styrene molecules (on the left) and ten OCH_3-styrene molecules (on the right) bond, computed for a silicon substrate cluster having the same cross section.

This behavior found in the simulations (lower current through the triple CF_3-styrene line than through the single CF_3-styrene line at low bias and the reduction in this contrast with increasing magnitude of the bias) is qualitatively similar to that seen experimentally in Fig. 3(f). However, quantitatively the suppression of the current through the triple CF_3-styrene line at low bias is more pronounced in the experiment [Fig. 3(f)] than in the theoretical curve V of Fig. 14(b): a 0.2–0.3 nm difference in tip height at constant current [as between the triple and single CF_3-styrene lines in Fig. 3(f) at low bias] normally corresponds to approximately a 2–3 orders of magnitude change in current at constant tip height in STM experiments.

Part of this difference between the simulation and experiment may be due to the unknown microscopic details of the STM tip, which are known to influence the height contrast between CF_3-styrene and OCH_3-styrene lines as is discussed

in Sec. II and can be seen in Fig. 2. However, the limited size of the model system for which the present simulations could be carried out[67] is clearly responsible for at least a part of the difference between the experimental and theoretical findings: while the downward electrostatic shift of the Si orbital energies [as indicated by the solid black curve in Fig. 14(c)] is clearly larger under the triple than the single CF_3-styrene line, it is evident that the eight molecule *single* CF_3-styrene line modeled is not long enough for the electrostatic potential in the silicon under the single CF_3-styrene line to reach a plateau with increasing distance from the junction with the triple CF_3-styrene line, i.e., the electrostatic influence of the triple row of molecular dipoles of the triple CF_3-styrene line is clearly being strongly felt under much of the single CF_3-styrene line as well, resulting in diminished contrast in the calculated current between the single and triple CF_3-styrene lines relative to that which may be expected in larger model systems. In this regard it is instructive to compare the electrostatic profile in the silicon under the single-triple CF_3-styrene heterostructure with that for a somewhat longer *single* file CF_3-styrene/OCH_3-styrene heterostructure shown by the dashed black curve in Fig. 14(c): for the latter heterostructure the potential profile in the silicon under the CF_3-styrene line (which is on the left) does show a pronounced plateau where the value of the electrostatic potential is close to that for the single-triple CF_3-styrene heterostructure under the *end* of the single CF_3-styrene line that is *furthest* from the triple CF_3-styrene line.

In comparing theory with experiment it is noted that there is also contrast between the tip currents calculated for tip positions over the three molecular rows within the triple row structure: the calculated current for the tip over the leftmost molecular row in Fig. 14(a) for the same tip height and bias as for plot V of Fig. 14(b) is shown by the dashed curve at the bottom of Fig. 14(b): the current over the left molecular row is smaller than over the center row of the triple structure (plot V). The calculated current over the rightmost row of Fig. 14(a) (not shown) is intermediate between that for the left and center rows. These results suggest that stronger contrast between the single CF_3-styrene line and parts of the triple CF_3-styrene than is seen in plot V of Fig. 14(b) may be possible theoretically. However, calculations for larger silicon clusters than were feasible in this study are required to eliminate possible cluster edge effects and develop a better understanding of this issue.

If the magnitude of the negative substrate bias is increased still further, well beyond that for current plot L in Fig. 14(b), the STM current through the single CF_3-styrene line is predicted by the present simulation to begin to increase more rapidly than that through the central line of the triple CF_3-styrene structure. This is seen in curve H of Fig. 14(b) where the current through the single CF_3-styrene line is again much larger than that through the triple CF_3-styrene line. This effect can be understood by considering the red curve (Ph) in Fig. 14(c): this shows the average of E_n over the six carbon atoms of the benzene ring of each molecule of the long CF_3-styrene row. This is higher for the single CF_3-styrene line than for the triple CF_3-styrene line. Therefore the molecular HOMO levels for the molecules in the single CF_3-styrene line are higher in energy than those for molecules in the center row of the triple CF_3-styrene line. Consequently the molecular HOMO levels for the molecules in the single CF_3-styrene line are crossed by the Fermi level of the STM tip at lower magnitudes of the negative substrate bias than for molecules in the triple CF_3-styrene line which results in the renewed enhancement of the current through the single CF_3-styrene line relative to the triple CF_3-styrene line seen in curve H of Fig. 14(b). No recovery of stronger contrast between the single and triple CF_3-styrene lines at stronger negative substrate bias is seen experimentally in Fig. 3(f) indicating that even for the strongest negative substrate bias values realized in these experiments the STM tip Fermi level remains well above the CF_3-styrene HOMO levels even for the molecules in the single CF_3-styrene line. This is consistent with our experimental findings for the CF_3-styrene/OCH_3-styrene heterostructures where no acceleration of the increase in the apparent height of the CF_3-styrene with bias at strong negative substrate bias (that would be indicative of the STM tip Fermi level crossing the CF_3-styrene HOMO) was observed.

VIII. DISCUSSION

The present experimental and theoretical work has begun to explore how electric fields emanating from molecules influence electrical conduction through other molecules in their close vicinity and in the underlying substrate.

In this work we have employed density-functional calculations only to estimate the electrostatic potential throughout the system in its electronic ground state, an application of density-functional theory that is believed to be soundly based at the fundamental level. The phenomena that we report on here can be understood *qualitatively* by considering just the results of these electrostatic calculations as summarized in Figs. 8 and 14(c). Transport calculations are however necessary to translate the electrostatics into current profiles that can be compared with the experimental STM data. As is discussed in Sec. III A, transport calculations that incorporate electronic structures obtained entirely from density-functional theory, although popular, are not soundly based and are often misleading, especially for molecules on semiconductors. We therefore base our transport calculations instead on electronic structures obtained from semiempirical tight-binding models modified to include the density-functional-theory-based ground-state electrostatic potentials.

Our theoretical modeling indicates the observed low bias filled-state current enhancement in the interfacial OCH_3-styrene molecules to be due to the collective effect of the electric-dipole fields generated by the OCH_3 groups of the OCH_3-styrene chain when the OCH_3 groups are aligned preferentially so that their carbon atoms are further from the heterojunction than their oxygen atoms, as they are, for example, in Fig. 9(a). It is plausible that structures of this sort are prevalent in these systems since some of them should be favored for molecules subject to a weak net mutual steric repulsion as is discussed in Sec. IV A. However the resolution of our experimental STM data which was taken at room temperature is not sufficient to determine independently whether or not the molecular chains have structural

order of this sort. Furthermore it is apparent from a comparison of our experimental data and theoretical results that the CF_3 groups in the CF_3-styrene molecules must be spinning rapidly enough on their axes that only an average over many conformations of these molecules is being observed in the STM images. Similarly it seems possible that many conformations of the OCH_3-styrene molecules are being averaged over rapidly in the STM imaging and that the above alignment of the OCH_3 groups is simply more commonly present than other structures, such as that in Fig. 9(b) for which the apparent height enhancement should be near the end of the OCH_3-styrene chain that is remote from the junction.

The behavior of the imaging height enhancement that we observe experimentally with increasing negative substrate bias is also consistent with the predictions of our theoretical model of this phenomenon.

Under positive substrate bias simulations indicate that height enhancement near the junction should also occur but should in this case be confined to only a single molecule. The location of the predicted height enhancement under positive substrate bias is sensitive to the details of the local molecular geometry in its vicinity that are expected to fluctuate rapidly at room temperature. Thus definitive observation of this effect will most likely require cryogenic experimental work.

The work reported here has succeeded in identifying transport phenomena occurring at molecular length scales that can reasonably be attributed to electric fields emanating from polar molecules impinging on other nearby molecules and on the underlying substrate, and in developing some insights into the detailed physical mechanisms that may be involved. As has been discussed in Sec. I these phenomena may ultimately find device applications, such as molecular switches in which the current through a molecule is switched by conformational changes in another nearby molecule and/or devices in which conduction through a semiconductor substrate is controlled with the help of molecules at its surface.

However further experimental and theoretical work is needed in order to better understand and ultimately control such phenomena.

ACKNOWLEDGMENTS

This research was supported by the Canadian Institute for Advanced Research, NSERC, iCORE, and the NRC. P.G.P. wishes to thank NRC-INMS for support. Some numerical computations presented in this work were performed on WestGrid computing resources, which are funded in part by the Canada Foundation for Innovation, Alberta Innovation and Science, BC Advanced Education, and the participating research institutions. WestGrid equipment is provided by IBM, Hewlett Packard, and SGI. We have benefited from discussions with G. DiLabio and from the technical expertise of D. J. Moffatt and M. Cloutier.

*Present address: Institute for National Measurement Standards, NRC, Ottawa, Ontario, Canada K1A 0R6.

[1] A. Troisi and M. A. Ratner, Small **2**, 172 (2006).
[2] N. J. Tao, Nat. Nanotechnol. **1**, 173 (2006).
[3] G. Kirczenow, in *The Oxford Handbook of Nanoscience and Technology*, edited by A. V. Narlikar and Y. Y. Fu (Oxford University Press, London, UK, 2009).
[4] L. Venkataraman, J. E. Klare, C. Nuckolls, M. S. Hybertsen, and M. L. Steigerwald, Nature **442**, 904 (2006).
[5] L. Venkataraman, Y. S. Park, A. C. Whalley, C. Nuckolls, M. S. Hybertsen, and M. L. Steigerwald, Nano Lett. **7**, 502 (2007).
[6] P. G. Piva, G. A. DiLabio, J. L. Pitters, J. Zikovsky, M. Rezeq, S. Dogel, W. A. Hofer, and R. A. Wolkow, Nature (London) **435**, 658 (2005).
[7] K. R. Harikumar, J. C. Polanyi, P. A. Sloan, S. Ayissi, and W. A. Hofer, J. Am. Chem. Soc. **128**, 16791 (2006).
[8] P. G. Piva, R. A. Wolkow, and G. Kirczenow, Phys. Rev. Lett. **101**, 106801 (2008).
[9] G. P. Lopinski, D. D. M. Wayner, and R. A. Wolkow, Nature (London) **406**, 48 (2000).
[10] P. Delaney and J. C. Greer, Phys. Rev. Lett. **93**, 036805 (2004).
[11] N. Sai, M. Zwolak, G. Vignale, and M. Di Ventra, Phys. Rev. Lett. **94**, 186810 (2005).
[12] C. Toher, A. Filippetti, S. Sanvito, and K. Burke, Phys. Rev. Lett. **95**, 146402 (2005).
[13] P. Darancet, A. Ferretti, D. Mayou, and V. Olevano, Phys. Rev. B **75**, 075102 (2007).
[14] F. Evers and K. Burke, in *Nano and Molecular Electronics Handbook*, edited by S. E. Lyshevski (Taylor and Francis, Boca Raton, 2007), p. 24-1.
[15] S. H. Ke, H. U. Baranger, and W. T. Yang, J. Chem. Phys. **126**, 201102 (2007).
[16] C. D. Pemmaraju, T. Archer, D. Sánchez-Portal, and S. Sanvito, Phys. Rev. B **75**, 045101 (2007).
[17] E. Prodan and R. Car, Phys. Rev. B **76**, 115102 (2007).
[18] S. Y. Quek, J. B. Neaton, M. S. Hybertsen, E. Kaxiras, and S. G. Louie, Phys. Rev. Lett. **98**, 066807 (2007).
[19] M. Koentopp, C. Chang, K. Burke, and R. Car, J. Phys.: Condens. Matter **20**, 083203 (2008), and references therein.
[20] K. S. Thygesen and A. Rubio, J. Chem. Phys. **126**, 091101 (2007); Phys. Rev. B **77**, 115333 (2008).
[21] C. Toher and S. Sanvito, Phys. Rev. Lett. **99**, 056801 (2007); Phys. Rev. B **77**, 155402 (2008).
[22] K. S. Thygesen, Phys. Rev. Lett. **100**, 166804 (2008).
[23] P. Hohenberg and W. Kohn, Phys. Rev. **136**, B864 (1964).
[24] P. E. Kornilovitch, A. M. Bratkovsky, and R. S. Williams, Phys. Rev. B **66**, 245413 (2002).
[25] E. G. Emberly and G. Kirczenow, Phys. Rev. Lett. **91**, 188301 (2003).
[26] A. Troisi and M. A. Ratner, Nano Lett. **4**, 591 (2004).
[27] J. J. de Jonge, M. A. Ratner, and S. W. de Leeuw, J. Phys. Chem. C **111**, 3770 (2007).
[28] J. J. Boland, Surf. Sci. **261**, 17 (1992).
[29] G. A. DiLabio, P. G. Piva, P. Kruse, and R. A. Wolkow, J. Am. Chem. Soc. **126**, 16048 (2004).
[30] X. Tong, G. A. DiLabio, O. J. Clarkin, and R. A. Wolkow, Nano

Lett. **4**, 357 (2004).
[31] P. Kruse, E. R. Johnson, G. A. DiLabio, and R. A. Wolkow, Nano Lett. **2**, 807 (2002).
[32] Certain substituents have been found to hinder the line growth process, and on occasion successful heterowire formation has been observed to depend on deposition sequence.
[33] L. P. Hammett, J. Am. Chem. Soc. **59**, 96 (1937).
[34] G. A. DiLabio, D. A. Pratt, and J. S. Wright, Chem. Phys. Lett. **311**, 215 (1999), and references therein.
[35] A. Y. Anagaw, R. A. Wolkow, and G. A. DiLabio, J. Phys. Chem. C **112**, 3780 (2008).
[36] H. Raza, K. H. Bevan, and D. Kienle, Phys. Rev. B **77**, 035432 (2008).
[37] G. Kirczenow, P. G. Piva, and R. A. Wolkow, Phys. Rev. B **72**, 245306 (2005).
[38] D. M. Cyr, B. Venkataraman, G. W. Flynn, A. Black, and G. M. Whitesides, J. Phys. Chem. **100**, 13747 (1996).
[39] J. R. Hahn and W. Ho, Phys. Rev. Lett. **87**, 196102 (2001).
[40] See the discussion of Figs. 1(b) and 1(d) in Sec. II for an explanation of why the OCH_3-styrene images higher than the CF_3-styrene at strong negative substrate bias and why the height of the OCH_3-styrene saturates in that regime.
[41] W. Kohn and L. J. Sham, Phys. Rev. **140**, A1133 (1965).
[42] J. Buker and G. Kirczenow, Phys. Rev. B **78**, 125107 (2008).
[43] T. Rakshit, G.-C. Liang, A. W. Ghosh, and S. Datta, Nano Lett. **4**, 1803 (2004).
[44] K. H. Bevan, F. Zahid, D. Kienle, and H. Guo, Phys. Rev. B **76**, 045325 (2007).
[45] R. Hoffmann, J. Chem. Phys. **39**, 1397 (1963).
[46] J. H. Ammeter, H.-B. Bürgi, J. C. Thibeault, and R. Hoffmann, J. Am. Chem. Soc. **100**, 3686 (1978) implemented in the YAeHMOP numerical package by G. A. Landrum and W. V. Glassey.
[47] S. Datta, W. Tian, S. Hong, R. Reifenberger, J. I. Henderson, and C. P. Kubiak, Phys. Rev. Lett. **79**, 2530 (1997).
[48] E. G. Emberly and G. Kirczenow, Phys. Rev. Lett. **87**, 269701 (2001).
[49] E. G. Emberly and G. Kirczenow, Phys. Rev. B **64**, 235412 (2001).
[50] J. G. Kushmerick, D. B. Holt, J. C. Yang, J. Naciri, M. H. Moore, and R. Shashidhar, Phys. Rev. Lett. **89**, 086802 (2002).
[51] D. M. Cardamone and G. Kirczenow, Phys. Rev. B **77**, 165403 (2008); AIP Conf. Proc. **995**, 135 (2008).
[52] J. Cerdá and F. Soria, Phys. Rev. B **61**, 7965 (2000).
[53] D. Kienle, K. H. Bevan, G.-C. Liang, L. Siddiqui, J. I. Cerdá, and A. W. Ghosh, J. Appl. Phys. **100**, 043715 (2006).
[54] The GAUSSIAN03 package with the B3PW91 density functional and Lanl2DZ basis set was used.
[55] E. G. Emberly and G. Kirczenow, Chem. Phys. **281**, 311 (2002), Appendix A.
[56] As in Ref. 37, in the present model the approximation is made that the entire potential drop V due to the applied bias occurs within the vacuum gap between the STM tip and molecule. This is a physically reasonable approximation since this gap is the weakest electrostatic and electronic link between the source and drain electrodes in STM experiments. It is also qualitatively consistent with published self-consistent calculations such as those of Bevan *et al.* (Ref. 57) who found that under bias the energies of the molecular levels of molecules adsorbed on a silicon surface and probed by an STM tip track the energies of the silicon band edges much more accurately than they do the electrochemical potential of the STM tip. We also note that unlike in the controversial resonant tunneling models of negative differential resistance (NDR) in molecules on silicon (Refs. 43 and 57) movement of a molecular level under applied bias across a silicon band edge into the silicon band gap does not occur in the present theory and there is no experimental or theoretical evidence suggesting that it may be occurring in the present system.
[57] K. H. Bevan, D. Kienle, H. Guo, and S. Datta, Phys. Rev. B **78**, 035303 (2008).
[58] The temperature T in the Fermi functions was set to 0 K in the calculations reported here.
[59] The numerical implementation of the GAUSSIAN98 package was used.
[60] See the inset of Fig. 1(d) of Ref. 8 for a representative example of the calculated densities of states of the HOMO bands for the OCH_3-styrene and CF_3-styrene molecules in a CF_3-styrene/OCH_3-styrene heterostructure on silicon.
[61] J.-H. Cho, D.-H. Oh, and L. Kleinman, Phys. Rev. B **65**, 081310(R) (2002).
[62] Image made with MACMOLPLOT program of B. M. Bode and M. S. Gordon, J. Mol. Graphics Modell. **16**, 133 (1998).
[63] The units of current are arbitrary principally because only a small number of atomic layers of the Si substrate are included in the present model.
[64] The very strong current contrast in curves E and H of Fig. 6 between the OCH_3-styrene chain and all or part of the CF_3-styrene chain is due in part to the resonant electron transmission through molecules via the molecular LUMO states of the CF_3-styrene being much stronger than the tunneling mechanism responsible for electron transmission through the OCH_3-styrene molecules. Furthermore, due to the differing electrostatic dipoles of the CF_3-styrene and OCH_3-styrene molecules the silicon conduction-band edge in the surface silicon layers under the OCH_3-styrene molecules is locally higher than it is under the CF_3-styrene molecules. This tends to weaken the current through the OCH_3-styrene relative to CF_3-styrene in empty-state imaging and thus also contributes to the strong current contrast.
[65] In our STM experiments imaging of the CF_3-styrene/OCH_3-styrene molecular heterowires in this very low bias regime was rarely possible, as is discussed in Sec. III B.
[66] Plots L and V in Fig. 4(b) of Ref. 8 are at the same values of the bias but for a tip trajectory 0.1 nm lower that in Fig. 14(b) of the present paper. The *lateral* location of the tip trajectory for plots L, V, and H in Fig. 14(b) was chosen so as to maximize the calculated current along the (straight line) trajectory in plot L in both the single and triple molecular chain regions in order to accurately reflect the current contrast between different parts of the trajectory. Such optimization was not carried out in Fig. 4(b) of Ref. 8.
[67] We include 423 Si atoms and 936 other atoms in our density-functional calculations of the electrostatic potentials in the single-triple row CF_3-styrene heterostructure on silicon.